Polar Aerosol Atmospheric Rivers: Detection, Characteristics, and Potential Applications

Rémy Lapere, Jennie L Thomas, Vincent Favier, Hélène Angot, Julia Asplund, Annica M L Ekman, Louis Marelle, Jean-Christophe Raut, Anderson Da Silva, Jonathan D Wille, et al.

JGR Atmospheres

RESEARCH ARTICLE
10.1029/2023JD039606

Polar Aerosol Atmospheric Rivers: Detection, Characteristics, and Potential Applications

Rémy Lapere[1], Jennie L. Thomas[1], Vincent Favier[1], Hélène Angot[1], Julia Asplund[2,3], Annica M. L. Ekman[3,4], Louis Marelle[5], Jean-Christophe Raut[5], Anderson Da Silva[5], Jonathan D. Wille[6], and Paul Zieger[2,3]

[1]Université Grenoble Alpes, CNRS, INRAE, IRD, Grenoble INP, IGE, Grenoble, France, [2]Department of Environmental Science, Stockholm University, Stockholm, Sweden, [3]Department of Meteorology, Stockholm University, Stockholm, Sweden, [4]Bolin Center for Climate Research, Stockholm, Sweden, [5]LATMOS/IPSL, Sorbonne Université, UVSQ, CNRS, Paris, France, [6]Institute for Atmospheric and Climate Science, ETH Zurich, Zurich, Switzerland

Abstract Aerosols play a key role in polar climate, and are affected by long-range transport from the mid-latitudes, both in the Arctic and Antarctic. This work investigates poleward extreme transport events of aerosols, referred to as polar aerosol atmospheric rivers (p-AAR), leveraging the concept of atmospheric rivers (AR) which signal extreme transport of moisture. Using reanalysis data, we build a detection catalog of p-AARs for black carbon, dust, sea salt and organic carbon aerosols, for the period 1980–2022. First, we describe the detection algorithm, discuss its sensitivity, and evaluate its validity. Then, we present several extreme transport case studies, in the Arctic and in the Antarctic, illustrating the complementarity between ARs and p-AARs. Despite similarities in transport pathways during co-occurring AR/p-AAR events, vertical profiles differ depending on the species, and large-scale transport patterns show that moisture and aerosols do not necessarily originate from the same areas. The complementarity between AR and p-AAR is also evidenced by their long-term characteristics in terms of spatial distribution, seasonality and trends. p-AAR detection, as a complement to AR, can have several important applications for better understanding polar climate and its connections to the mid-latitudes.

Plain Language Summary The extreme transport of aerosol-containing air masses, from the mid-latitudes to the polar regions, can be characterized and quantified by leveraging polar Aerosol Atmospheric Rivers (p-AARs). This is similar to the Atmospheric Rivers (ARs) which carry large amounts of water to the poles and affect the overall stability of polar ecosystems. In this work, we establish a detection algorithm for p-AARs and evaluate it for different well-known aerosol intrusions or AR events. The areas most affected by p-AARs are described, their trends are investigated and we discuss the potential applications of p-AAR detection for a better understanding of polar climate.

Key Points:

- A catalog of polar aerosol atmospheric rivers (p-AAR) is provided for 1980–2022 by adapting an atmospheric river (AR) detection scheme
- Important p-AAR events, representing rapid poleward transport of aerosol-enriched air masses, are presented
- Combining AR and p-AAR can improve our understanding of the links between mid- and polar-latitudes, in the past, present and future climate

Correspondence to:
R. Lapere and J. L. Thomas,
remy.lapere@univ-grenoble-alpes.fr;
jennie.thomas@univ-grenoble-alpes.fr

Citation:
Lapere, R., Thomas, J. L., Favier, V., Angot, H., Asplund, J., Ekman, A. M. L., et al. (2024). Polar aerosol atmospheric rivers: Detection, characteristics, and potential applications. *Journal of Geophysical Research: Atmospheres*, *129*, e2023JD039606. https://doi.org/10.1029/2023JD039606

Received 7 JUL 2023
Accepted 26 DEC 2023

Author Contributions:
Conceptualization: Rémy Lapere, Jennie L. Thomas, Vincent Favier, Hélène Angot, Louis Marelle
Formal analysis: Rémy Lapere, Jennie L. Thomas, Julia Asplund
Methodology: Rémy Lapere, Jennie L. Thomas, Vincent Favier, Julia Asplund, Annica M. L. Ekman
Visualization: Rémy Lapere
Writing – original draft: Rémy Lapere, Jennie L. Thomas, Vincent Favier, Hélène Angot
Writing – review & editing: Julia Asplund, Annica M. L. Ekman, Louis Marelle, Jean-Christophe Raut, Anderson Da Silva, Jonathan D. Wille, Paul Zieger

1. Introduction

Polar regions are experiencing climate change more than any other region of the planet (Hall, 2004; Rantanen et al., 2022). Changes in aerosol emissions are significantly contributing to the recent Arctic warming, through the interaction of aerosols with clouds and radiation (Acosta Navarro et al., 2016; AMAP, 2021). This faster change is also impacted by the cloud phase feedback, which is influenced by aerosols (Tan & Storelvmo, 2019). In parallel, aerosols and clouds (and their interactions) comprise a large uncertainty in global climate predictions, including in the Arctic and Antarctic (Myhre et al., 2013; Szopa et al., 2021). In addition, the polar regions are largely snow and ice covered and one important polar climate feedback mechanism is through deposition of light absorbing aerosols (including dust and black carbon) which darkens these surfaces and accelerates melting/warming (Bond et al., 2013; Skiles et al., 2018). Therefore, it is critical to be able to estimate the aerosol budget in the polar regions, including the contribution from rapid transport from the mid-latitudes toward the poles (Schmale et al., 2021).

The aerosol lifecycle in the polar regions has specific characteristics compared to typical urban or remote regions found at mid-latitudes. Primary aerosol sources in the Arctic and Antarctic include sea spray from the open ocean, leads and blowing snow (Abbatt et al., 2019; Frey et al., 2020; Kirpes et al., 2019), dust from ice-free terrain (Amino et al., 2021; Bullard et al., 2016; Meinander et al., 2022), and some local anthropogenic emissions (Marelle et al., 2018; Roiger et al., 2015). Intrusions of aerosol-containing mid-latitude air masses contribute

significantly to the aerosol budget in the Arctic (J. L. Thomas et al., 2017; Zhao et al., 2022) and Antarctic (Jumelet et al., 2020), and may affect polar cloud properties with important climate implications (Dada et al., 2022; Shi et al., 2022). In the Arctic in winter and spring, the polar dome expands to include some parts of Europe, Eurasia, and North America, so that pollution from the mid-latitudes can be transported at low levels toward the Arctic, which is known as the Arctic Haze phenomenon (Barrie, 1986; Quinn et al., 2007). Aerosols are also transported from lower latitudes into the Arctic dome via three possible pathways: low-level transport followed by uplift upon reaching the dome and eventually descent, direct injection into the free troposphere at the source followed by long-range transport, or via mid-latitude cyclones transporting pollutants in the free troposphere into the Arctic (Stohl, 2006; M. A. Thomas et al., 2019). Several of these circulation types can be associated with warm air mass intrusions, as reviewed in Pithan et al. (2018), or the more extreme atmospheric rivers (AR), which also bring large quantities of moisture and precipitation to the polar regions (Gorodetskaya et al., 2014; Maclennan & Lenaerts, 2021; Turner et al., 2019).

ARs are defined as long filamentary bands of poleward moisture transport often embedded within the low-level jet ahead of an extratropical cyclone's cold front. They make a major contribution (90%) to the transport of water vapor from the interior of the tropics to the mid-latitudes and the poles, even though they cover only about 10% of the surface area; four or five AR in each hemisphere may therefore be sufficient to carry the majority of meridional flows across the globe (Nash et al., 2018; Zhu & Newell, 1998). ARs are low-frequency, high-impact events with major implications for the global hydrological cycle. They have been linked with flooding and drought busting (i.e., water system replenishment during dry spells) in the mid-latitudes (Lavers et al., 2012; Neiman et al., 2013; Ralph et al., 2019), and ice-sheet mass balance impacts in polar regions (Adusumilli et al., 2021; Mattingly et al., 2018; Wille et al., 2019, 2021, 2022). Due to their crucial role in the hydrological cycle, various global AR detection algorithms have been developed, as summarized for example, in the Atmospheric River Tracking Method Intercomparison Project (ARTMIP) program (Shields et al., 2018, 2022). ARs in the mid-latitudes have been shown to initiate the deposition of long-range transported dust and biological aerosols through ice riming when the AR moisture is forced upward through orographic or isentropic ascent (Creamean et al., 2013; Francis et al., 2022). Given the importance of AR for moisture transport, and the importance of aerosols for cloud formation, distinguishing clean and aerosol-containing ARs could be important for understanding precipitation, surface and cloud albedo, radiation and melting impact of ARs.

Inspired by the concept of ARs, Chakraborty et al. (2021, 2022) proposed the definition of aerosol atmospheric rivers (AARs) to characterize the rapid, large-scale transport of large quantities of aerosols. Chakraborty et al. (2021) developed an objective global algorithm to detect AARs and demonstrated that they play a crucial role in long-range transport pathways, accounting for a significant fraction (40%–80%) of global total aerosol transport over relatively few events (20–40 AAR days/year). These works demonstrated that AARs can be detected and are useful for investigating and quantifying aerosol transport.

For polar applications, it is important to adapt the detection of AARs to the specific characteristics of poleward transport. This is similar to the case of ARs, where there is a large spread in AR detection frequency between global and regional methods (Collow et al., 2022). Due to the lower moisture capacity of colder, polar atmospheres, most global AR detection algorithms tend to capture an overly broad swath of extratropical cyclone activity instead of the more characteristically intense meridional moisture transport seen in ARs. Thus a regional detection method is better suited for studying AR connections with modes of variability, especially around the Southern Ocean (Shields et al., 2022).

Here, we follow the development of the concept of AARs, from Chakraborty et al. (2021, 2022), but adapt the polar AR detection method developed by Wille et al. (2019) to do so, in order to identify polar oriented extreme transport of aerosols. These will be referred to as polar aerosol atmospheric rivers (p-AAR) hereafter. Leveraging this detection, we aim to answer the following scientific questions:

- What are the characteristics and climatology of p-AARs?
- How do p-AARs compare with ARs?
- Can p-AARs provide a moisture-independent characterization of atmospheric circulation during extreme poleward transport events?

In order to answer these questions, the paper is organized into the following sections. In Section 2, the algorithm and the input data used for AR and p-AAR detection are described. Then, we show case studies of major ARs and

p-AARs, validating the detection method and illustrating the interest of a combined approach to extreme transport events (Section 3). The climatology and characteristics of p-AAR in the Arctic and the Antarctic obtained with this algorithm are also presented in Section 3. Finally, we discuss the potential applications of this p-AAR catalog in Section 4.

2. Data and Methods

2.1. AR and p-AAR Detection Methods

The quantity of interest for p-AAR detection is the vertically integrated, meridional mass flux of aerosol (denoted v*IxT*), as described by Equation 1.

$$\mathrm{v}IxT = \int_{surface}^{top} V\,x\,dp \tag{1}$$

where V is the meridional wind speed, dp is the pressure level increment, and x is the transported quantity of interest (water vapor mixing ratio for AR, aerosol mixing ratio for p-AAR).

We focus on three key aerosol species for p-AARs including: black carbon (BC), dust (DU), and sea-salt (SS). These three species are selected because they are representative of different types of emission sources and processes, and cover most of the global mass of primary aerosols (Chin et al., 2002). Organic Carbon (OC) p-AARs are also considered for a case study although the climatology is not investigated in detail. For each time step, whenever a grid point has a v*IxT* directed poleward (i.e., positive for the Northern Hemisphere, negative for the Southern Hemisphere), it is considered a p-AAR-participating point provided that the v*IxT* value for this point is larger than the historical 97th percentile (P97) for the whole corresponding month over the 1980–2022 climatology (see Appendix A2 for more details). The choice of P97 is discussed in Section 3.1. When a continuous area (i.e., a contour) of p-AAR-participating points extends more than 20° in latitude, a p-AAR is detected. This detection scheme is adapted from Wille et al. (2019, 2021) and applied in this work both to integrated meridional fluxes of water vapor for the detection of ARs, and to integrated meridional fluxes of BC, DU, SS and OC for p-AARs. The suitability of the 20°-latitude extent criterion for p-AAR is discussed in Appendix A2. The validation of the adaptations compared to the original AR detection method is provided in Appendix A2.

This detection method is different from the one adopted by Chakraborty et al. (2021), owing to our need for a polar-adapted detection. The main differences between these two approaches are described in Appendix A3, along with a comparison of the climatologies given by the p-AAR and AAR catalogs, and examples of differences in detections based on case studies.

The definition of an AR consists in selecting extreme events based on considerations of extreme moisture transport amounts. The detection algorithms take into account an AR event by analyzing points where the meridional integrated vapor transport (v*IVT*) exceeds a threshold value. For AR detection, the threshold is taken at P97 here, as it matches best with the reference AR climatologies from Wille et al. (2019), with the MERRA-2 input data used here (described in Section 2.2), although Wille et al. (2019) used a P98 threshold instead. This is connected to different spatial resolutions and assumptions in the computation of v*IVT* (different vertical extent for the integration), as explained in Appendix A2.

Like for AR, a key parameter for a p-AAR detection methodology is the threshold for which grid cells are considered p-AAR-participating. There is no reason why the same number of events should be found for different aerosols. The definition of an AR or p-AAR event should therefore be based solely on an objective and independent statistical detection criterion, regardless of the aerosol type under consideration. For this reason, we recommend considering the same percentile for all aerosol types. In this work, we chose to remain consistent between the transport of moisture and aerosols in order to capture similar types of anomalous events, regardless of the transported quantity. As a result, the threshold P97 is also used for p-AARs.

The algorithms for AR and p-AAR detection described in this work are implemented in a Python3 Jupyter Notebook (Kluyver et al., 2016). This code leverages the contour detection offered by the Matplotlib library (Hunter, 2007), and the image analysis tools from the OpenCV library (Bradski, 2000) which provides an efficient way of masking 2-dimensional data. The corresponding detection catalogs for AR and p-AAR, based on MERRA-2 vertically

integrated fluxes at 1° × 1° spatial resolution (see Section 2.2) and covering the period 1980–2022, along with the processing and detection codes, are available at https://doi.org/10.5281/zenodo.8082768 (Lapere, 2023).

Using the definition described above, p-AARs can be seen as a selection of the most extreme aerosol transport events reaching high latitude that are long enough and with a poleward orientation. Regional and seasonal large-scale pollution transport, such as Arctic haze, is not detected as p-AAR due to the use of an extreme (P97), seasonal (monthly) and local (point by point) threshold, which filters out regularly occurring aerosol transport pathways. p-AARs are extreme transport events that are generated by strong blocking activity, similar to polar ARs (Wille et al., 2019), and they therefore have elongated, filament-like structures (see the detection catalog available at https://doi.org/10.5281/zenodo.8082768 (Lapere, 2023) and Figures in Section 3.2). Due to their shape and their similarity to polar ARs, we refer to these events as aerosol atmospheric rivers.

Mid-latitude AR/AAR detection algorithms traditionally use lower thresholds, for example, P85, and include additional constraints on length (i.e., greater than 2,000 km, which corresponds to our 20°-latitude criterion) and aspect ratio (greater than 2:1). Due to the nature of transport to the polar regions, Wille et al. (2019) found that by using a more selective threshold than P85, the additional aspect ratio criteria is not needed. The 2:1 aspect ratio is respected using our detection method with average length to width ratios of 2.3:1 and 2.4:1 for BC and DU p-AAR reaching 65°N, and 3.1:1 and 3.2:1 for BC and DU p-AAR reaching 65°S.

2.2. MERRA-2 Data

The data used for AR detection is the MERRA-2 hourly Vertically Integrated Diagnostics, *northward flux of atmospheric water vapor*. Similarly, the detection of p-AARs is performed using the MERRA-2 hourly Vertically Integrated Diagnostics, *dust/black carbon/sea salt/organic carbon column v-wind mass flux*. The MERRA-2 aerosol product was also used in Chakraborty et al. (2021, 2022) for AAR detection. These products are integrated fluxes over the whole atmospheric column (1000 hPa to 0.1 hPa). Additionally, large scale meteorological conditions (500 hPa geopotential height, 500 hPa winds and surface precipitation) associated with the case studies presented are extracted from the single-level MERRA-2 hourly reanalysis. Geopotential height anomalies are computed as the difference between the hourly values averaged over the considered event and the monthly mean climatology for the corresponding month. For these case studies, vertical profiles of aerosol and water mixing ratio are from the MERRA-2 hourly product on pressure levels. Total column mass concentration and surface concentration of aerosols, as well as aerosol optical thickness are from the MERRA-2 hourly single level aerosol assimilation product. All data sets are systematically re-gridded to the 1° × 1° spatial resolution and re-sampled to a 3-hourly time resolution. Monthly aerosol emission fluxes from MERRA-2 are also considered, for the 1980–2022 period. For readability, the references corresponding to these data sets are summarized as Global Modeling and Assimilation Office (GMAO) (2015a, 2015b, 2015c, 2015d, 2015e). Emissions of sea salt and dust in MERRA-2 are computed online at hourly resolution, while biomass burning emissions are daily inputs (Randles et al., 2017). Although no validation of MERRA-2 aerosols is carried out in this work, previous studies on polar aerosols have relied on MERRA-2 data and showed reasonable performance of this product at high latitudes (Böö et al., 2023; Xian et al., 2022; Zamora et al., 2022). In addition, the fact that the events presented in Section 3.2 are adequately captured by MERRA-2 suggests that this product is fit for the purpose of detecting extreme transport events of aerosols.

3. Results and Discussion

3.1. p-AAR Detection Thresholds

The sensitivity of the p-AAR detection to the threshold choice is tested in Figure 1a. With a P99 threshold, the fraction of grid points above 60°N or below 60°S which belong to a p-AAR is less than 0.2%, on average, for all aerosol species and both poles. With P97, this number increases to around 0.5%–1% for non SS species. For SS this number is lower, at 0.2%. As the threshold decreases, the number of p-AAR points increases, up to around 20% of the domain, on average, for a P65 threshold. This illustrates how strongly the detection depends on the selection of the threshold.

In Figure 1b, we look at the percentage of AR points, over the climatology, which are also p-AAR points (i.e., overlapping contours), using different p-AAR detection thresholds (but keeping P97 for ARs). We investigate this

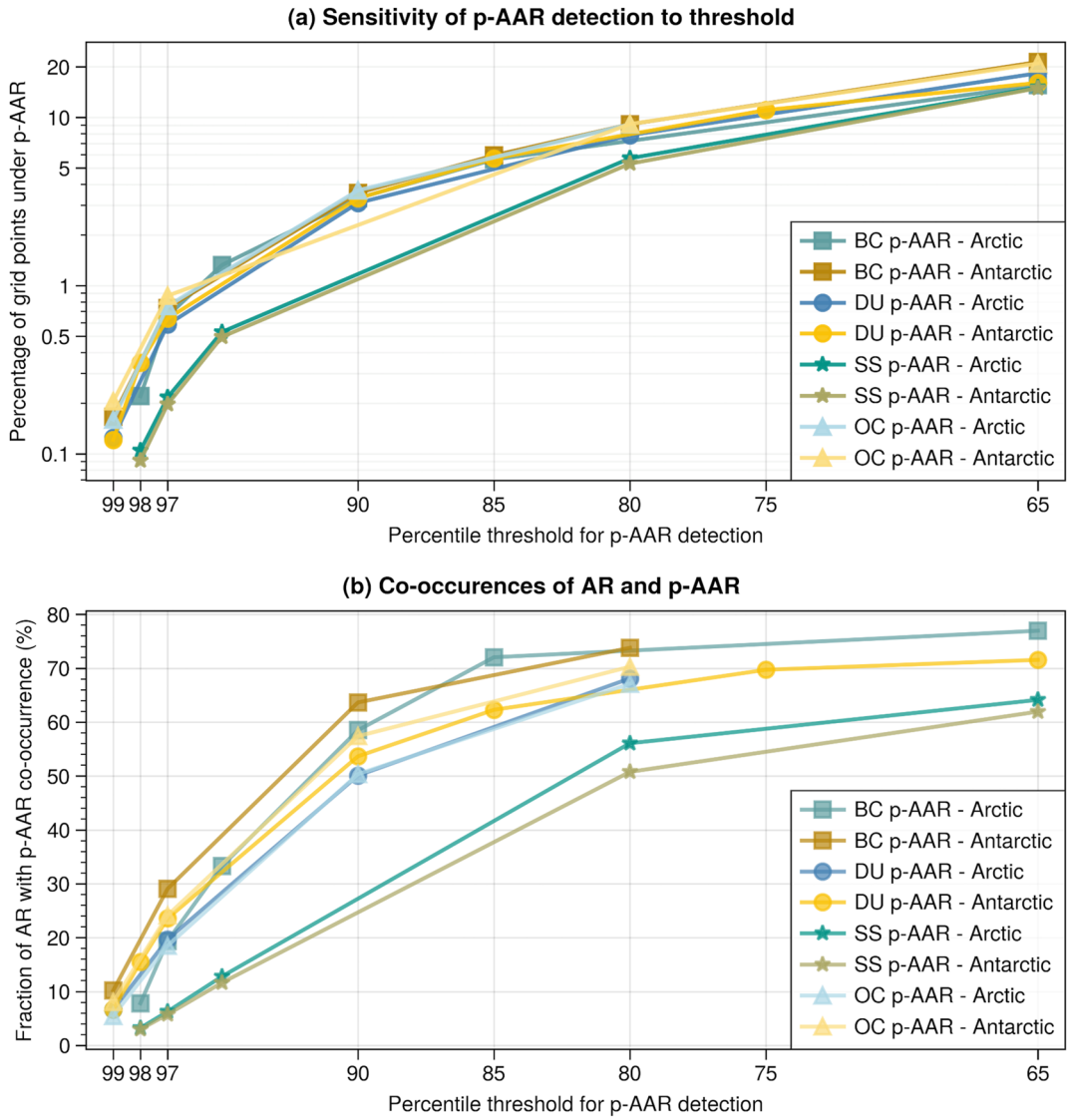

Figure 1. Polar Aerosol Atmospheric River detection - threshold sensitivity. (a) Average percentage of p-AAR grid points as a function of the detection threshold, for Black carbon (BC - squares), Dust (DU - circles), Sea salt (SS - stars) and Organic carbon (OC - triangles) p-AAR, in the Arctic (60°–85°N - blue) and the Antarctic (60°–85°N - yellow). (b) Fraction of Atmospheric River (AR) grid points with co-occurring p-AAR as a function of the p-AAR detection threshold.

sensitivity for BC, DU, SS, and OC, for the Arctic and the Antarctic, with similar conclusions for all, irrespective of the hygroscopic nature of the aerosol type. For percentiles above P85, the slope is steep and the number of co-located AR and p-AAR points varies strongly, between less than 5% for P99, and up to 70% for P85. For percentiles below P85, the number of co-occurrences starts to reach its asymptotic value of 70%–80%. This shows that no matter what percentile threshold is chosen for p-AARs, 20%–30% of AR grid cells cannot be described as p-AAR grid cells, and therefore belong to pristine (no aerosol) AR cases. This illustrates that while ARs and p-AARs may be similar (see Section 3.3), they describe different phenomena.

Figure 1 also shows that SS p-AARs behave differently from other p-AAR types. For similar detection thresholds, SS p-AAR are detected less often than for other aerosols, and also coincide less often with ARs. This can be connected to the relatively closer source of SS in polar regions compared to other aerosol sources. The DU and BC aerosols found at the poles mostly originate from the mid-latitudes, but SS is mainly emitted from open ocean areas, such as the Southern Ocean or North Atlantic and North Pacific, which are located closer to the poles. As

a result, the background SS is higher and the regional transport more frequent, which leads to a higher P97 and therefore lower frequency of SS p-AAR. The implications of this result are further discussed in the continuation.

3.2. Validation of the Detection With Case Studies

Here we study events of AR and large aerosol transport which were well monitored and documented in the literature, in order to assess if they are well captured by our detection algorithm. We analyze these case studies using both the AR and p-AAR detections and show the interest of adopting a combined analysis approach for a better understanding of extreme poleward transport events.

3.2.1. 2013 Asian Dust Transport to the Arctic

A dust transport event from Asia to the high Arctic, originating from the Gobi desert, was recorded in March 2013, which resulted in several days of enhanced pollution measured at Arctic stations (Zhao et al., 2022). Although this event was originally studied from the point of view of dust transport, the AR/p-AAR detection scheme developed in this study shows that extreme transport of other aerosols and water vapor also occurred simultaneously at these dates, along the same pathways, with AR, BC p-AAR and SS p-AAR detected in addition to the DU p-AAR (Figure 2). Figure A1 reveals that the DU transport was originally zonal above Asia, and turns poleward near the 180° longitude mark, where AR and p-AARs are detected, extending from 35°N to 90°N. This spatial pattern is consistent with the findings from Zhao et al. (2022). Figure A1 also shows that although the AR/p-AARs have similar spatial extents, they are associated with transport originating from different areas.

Based on the patterns in Figure A1, DU most likely comes from the Gobi desert, which was shown and discussed in Zhao et al. (2022) using backward trajectory analysis. BC, SS and water vapor likely originate from various source regions, different from DU according to Figure A1. Therefore, these similar AR/p-AAR detections actually connect different sources to the receptor region in the Arctic.

The vertical profiles associated with this transport event (Figure 2) reveal that the DU aerosols are transported in two layers, at around 700 hPa and 400 hPa. BC aerosols are found in the same 700 hPa layer, but not higher up in the atmosphere. In comparison, the SS aerosols and moisture along the transect are mostly found near the surface, below 800 hPa, in connection with more local sources of SS and moisture. The DU and BC transport pathway near 700 hPa is consistent with the transport mechanism from Asia due to lifting of air mass and slow descent in the Arctic due to radiative cooling, described in Stohl (2006), although the transect shown here is too short for this descent mechanism to be visible. The 400 hPa DU layer on the other hand can either come from longer range transport, or from the same source region and have been lifted higher up at another time, as illustrated by the back-trajectories in Roiger et al. (2011). Climatological zonal mean cross sections of BC in Wang et al. (2014) further indicate that the 400 hPa layer likely comes from sources located in South or East Asia or North Africa, while the 700 hPa layer most likely originates from Northern Asia or Northern Europe. This layer may also come from the generally excessive concentrations of DU in the polar free troposphere in MERRA-2 (Böö et al., 2023).

This event was of importance for the Arctic climate: Zhao et al. (2022) estimate that it contributed to a reduction of snow and ice albedo of around 2%, due to deposition of dust and soot. Therefore, quantifying the frequency of such events is critical for a better understanding of the Arctic climate. Moreover, this Asian dust transport event was recorded as a polar crossing event, with increases in particulate matter concentration as far as Alert, Canada (Zhao et al., 2022). Therefore, we would expect the DU p-AAR contour to reach this region. However, the p-AAR detection is, by design, unable to capture polar crossing events since the condition for the detection of a p-AAR is that the transport has to be directed toward the pole. This is a limitation of the current algorithm, which is also a limitation of polar AR detection methods. Similar polar-crossing aerosol transport events were also observed and studied in Sodemann et al. (2011); Raut et al. (2017), for example, which justifies improving current algorithms for a more comprehensive detection.

3.2.2. 2020 European Pollution Transport to the Arctic

In April 2020, an extreme aerosol transport event was recorded in the central Arctic (85°N, 15°E) during the international Multidisciplinary drifting Observatory for the Study of the Arctic Climate (MOSAiC) expedition (Dada et al., 2022; Shupe et al., 2022) which involved the Polarstern research vessel. Measurements showed strong, rapid increases in aerosol surface concentrations, including BC and OC. This event is well captured by our detection algorithm (Figure 3a "MOSAiC event"), with an AR detected on April 15, at the onset of the event,

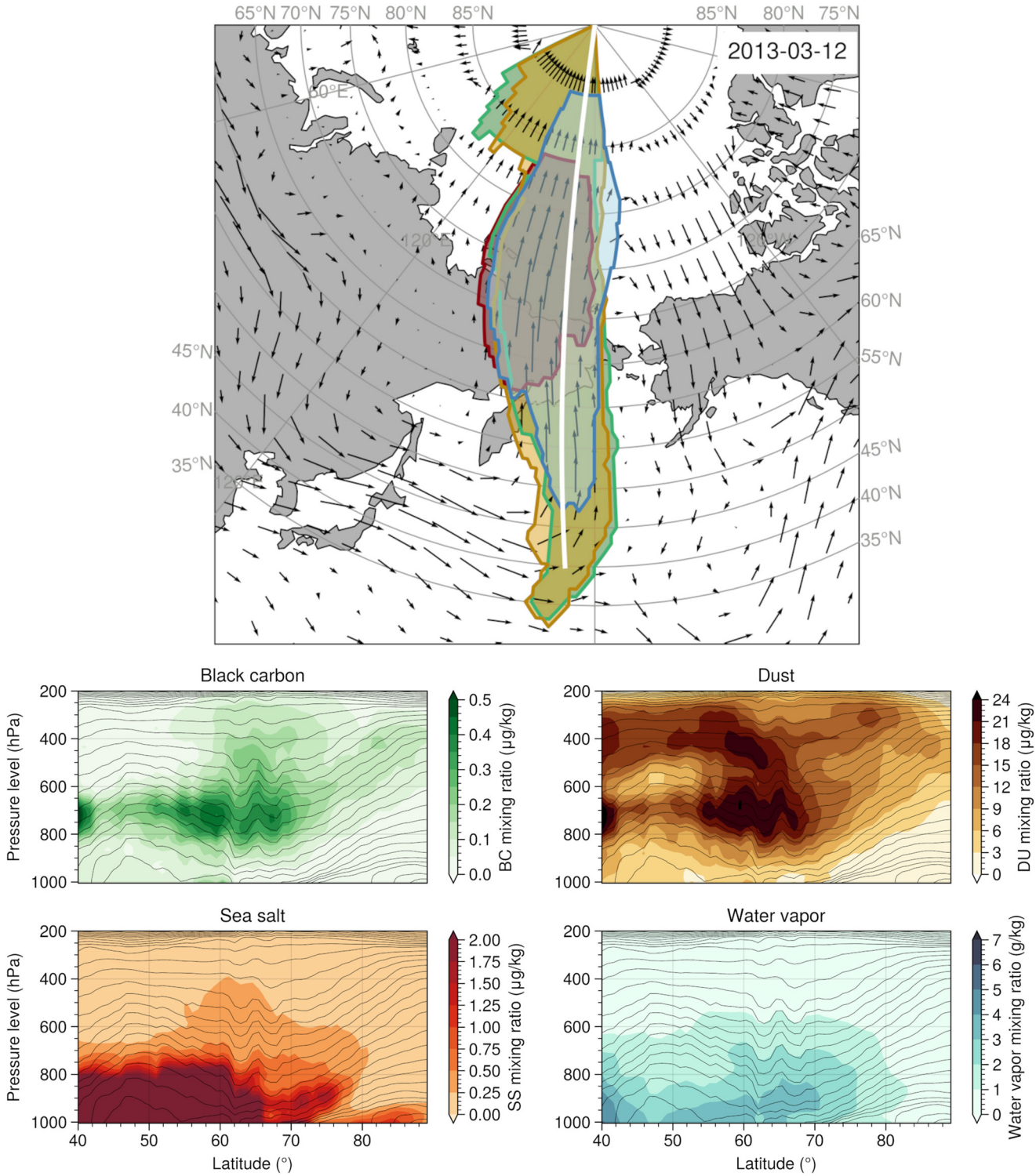

Figure 2. 2013-03-12 Asian dust transport to the high Arctic. Top: detection of Atmospheric River (AR - lightblue), Black carbon (BC - green), Dust (DU - yellow) and Sea salt (SS - red) polar Aerosol Atmospheric Rivers (p-AAR), and 500 hPa wind (arrows) on 2013-03-12. Bottom: vertical profiles of BC, DU, SS, and water vapor mixing ratio along the white transect in the top panel. Contours indicate constant levels of equivalent potential temperature (isentropes).

which was described as driven by a warm air mass intrusion by Dada et al. (2022). In parallel, a BC and an OC p-AAR are detected on the same day, lasting for 3 consecutive days, during which increased BC surface concentrations were recorded (Figure 3b). Dada et al. (2022) also noted increased concentrations of OC in addition to

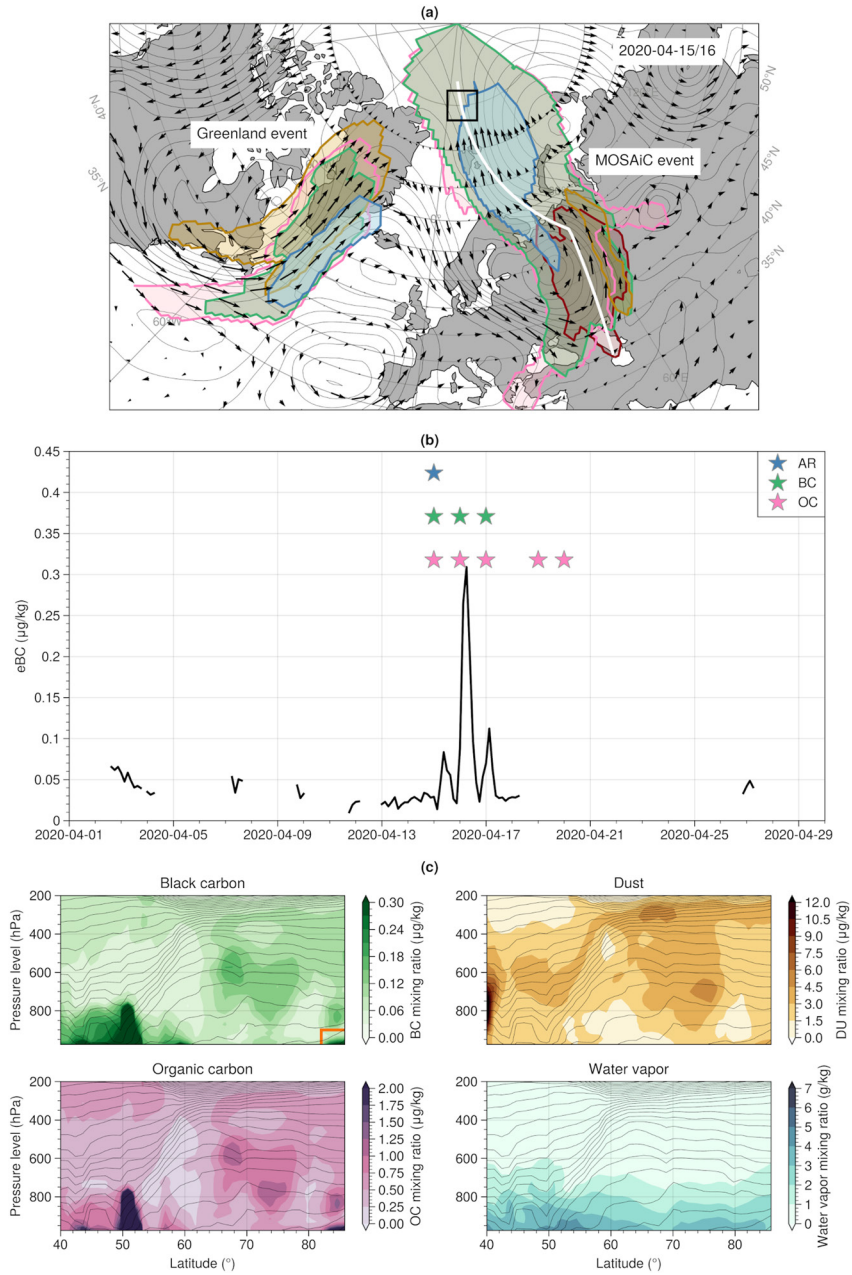

Figure 3. 2020-04-15 pollution transport to the Arctic during MOSAiC. (a) Synoptic circulation and Atmospheric River (AR) and polar Aerosol Atmospheric River (p-AAR) detection on 2020-04-15/16. Blue shade is AR, green shade is Black carbon (BC) p-AAR, pink shade is Organic carbon (OC) p-AAR, yellow shade is Dust (DU) p-AAR, red shade is Sea salt (SS) p-AAR. Wind field (arrows) and geopotential height anomalies (contours) are superimposed on the detections. The location of the ship is indicated by the black square. (b) Time series of equivalent BC measured onboard the ship (black line - data from Heutte et al. (2022) converted from concentration to mixing ratio assuming air density of 1.2922 kg m^{-3}) and corresponding AR/p-AAR daily detections (stars - blue is AR, green is BC p-AAR, pink is OC p-AAR) in the ship area (black square in panel a). (c) Vertical profiles of aerosol and water vapor mixing ratio along the white transect represented in panel a. The orange rectangle indicates the area where the ship was located. Contours indicate constant levels of equivalent potential temperature (isentropes).

BC, with which our OC p-AAR detection is also consistent. Figure 3c further shows that MERRA-2 captures this event adequately, with BC surface mixing ratios rising up to 0.3 µg kg^{-1} both in the observations and the reanalysis at the location of the ship (orange square in Figure 3c).

The vertical profiles associated with this event reveal that the transport of aerosols occurs at several altitudes (Figure 3c). The large quantities of BC and OC close to the surface are consistent with the observations from Dada et al. (2022) that low-altitude transport of air masses from northern Eurasia explained the measured increase in aerosols at the location of the Polarstern. The secondary aerosol layer higher up, around 600 hPa, is more likely connected to transport from eastern and southern Asian sources, which dominate the high-altitude transport to the Arctic in spring (Xu et al., 2017). Similar to the Asian dust case presented in Section 3.2.1, moisture is transported close to the surface, below 800 hPa.

Dada et al. (2022) highlight the importance of this event with respect to aerosol-cloud interactions, and therefore climate, with an observed strong increase of cloud condensation nuclei (CCN) concentrations during the intrusion. This event was observed during the MOSAiC expedition, with a unique set of in situ and remote sensing measurements available. However, Figure 3a shows that at the same time, another major combined AR/p-AAR event reached Greenland ("Greenland event"). First, a DU p-AAR is detected, which can affect the formation and characteristics of mixed-phase clouds given the important role of dust as ice nucleating particle (INP) (Murray et al., 2012). Second, because an AR is also associated with the BC and DU p-AAR, light-absorbing aerosols were likely deposited to the Greenland ice sheet by wet scavenging. Events like these may impact the albedo of the Greenland ice sheet through deposition of light-absorbing impurities, thereby contributing to accelerate the melting of the cryosphere, through the snow albedo feedback (Skiles et al., 2018). The precise impact of such p-AAR events needs to be studied as well, despite the lack of in situ measurements. In summary, this case study shows how the use of p-AAR detection can form the basis of more systematic studies of such extreme aerosol transport events and their impact on polar climate.

3.2.3. 2002 Antarctic Peninsula AR

On 19 February 2002, a major AR event was detected in the Antarctic Peninsula (AP) and was connected to the final collapse of the Larsen B ice shelf (Wille et al., 2022). This event is also detected as a DU p-AAR (Figure 4 presents the synoptic situation during this event). However, the DU p-AAR (yellow shade) and AR (blue shade) have different spatial coverage (Figure 4c). According to our catalog, an AR is detected in the southern Pacific Ocean, which does not extend further south than the tip of South America. However, when using the AR occurrences detected by Wille et al. (2022) with their algorithm based on integrated water vapor (*IWV*) values instead of v*IVT*, the AR contour (pink shade) made landfall in good agreement with the area where the highest rainfall rates were observed (Figure 4d), except for the southwestern precipitation area over Ellsworth land.

For the event depicted in Figure 4, the highest water vapor amounts are simulated in a more zonal flow and are divorced from the strongest meridional flow near the extratropical cyclone center (Figure 4d). This orientation lowered the meridional moisture transport below the detection threshold over the AP. As the *IWV* AR detection is independent of moisture transport direction, the algorithm detects an AR extending further poleward within the region of zonal winds.

All of the precipitation reaching the AP is within the DU p-AAR contour. In this case, with an AR-only approach, whether using v*IVT* or *IWV*, the precipitation in Ellsworth land is not associated to the transport event, but by combining v*IVT* AR with *IWV* AR and DU p-AAR the whole precipitation event can be traced back to the extreme long-range transport of air masses. Precipitation is a critical mass source for the ice sheet (Lenaerts et al., 2019). However, rainfall brought by AR can cause melt-albedo feedback and enhance snow melt (Box et al., 2022). As a result, precipitation events reaching the ice sheet, including the water phase, are of major importance. Therefore, it is critical to be able to capture the whole precipitation event in this case to better identify the underlying sources and transport pathways, and connect to the type of precipitation.

For this event, the DU aerosol and moisture had different source regions. The DU p-AAR most likely originated from Australia (Figure 4a), while the moisture that contributed to the AR comes from the central tropical Pacific area (Figure 4b), the region where the strongest ARs affecting the AP are generated, as described in Clem et al. (2022). After traveling above the Pacific Ocean, these two air masses generating the AR and p-AAR meet in a confluent manner, near 40°S–110°W and converge afterward. This shows how an AR and p-AAR corresponding to the same event can connect the impacted region to different source areas and therefore transport processes. This case can also illustrate how ARs and p-AARs partly follow the same trajectories (here they overlap at around 35°S), but later diverge (here the p-AAR goes further poleward than the AR and with a more meridional axis) as

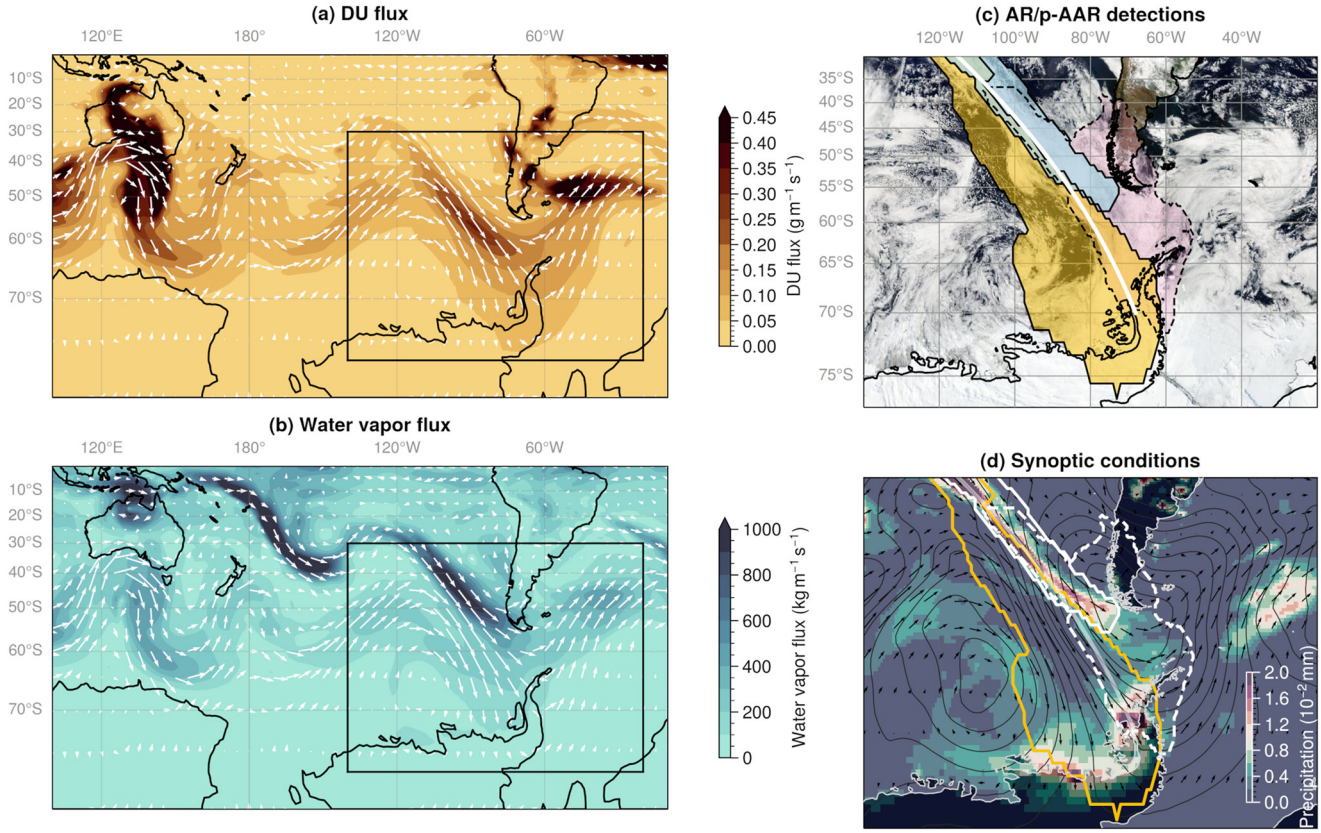

Figure 4. 2002-02-19 Antarctic Peninsula Atmospheric River. Vertically integrated Dust (DU) (a) and water vapor (b) flux (zonal and meridional) from MERRA-2 on 2002-02-19 (colormap) and associated 500 hPa wind field (arrows). (c) Detected Atmospheric River (AR - blue shade) and DU polar Aerosol Atmospheric River (p-AAR - yellow shade) near the Antarctic Peninsula on 2002-02-19. Pink shade with dashed contour is the AR detected in Wille et al. (2022) using Integrate Water Vapor (*IWV*) instead of meridional Integrated Vapor Transport (v*IVT*). Background: Moderate-Resolution Imaging Spectroradiometer (MODIS) Terra corrected reflectance, downloaded from the Earth Observing System Data and Information System (EOSDIS) Worldview (NASA, 2013). (d) Detected AR (white contour), DU p-AAR (yellow contour) and *IWV* AR (white dashed contour), 500 hPa geopotential height anomaly (black contours), 500 hPa winds (arrows), and precipitation (colormap). The extent of the right-hand panels corresponds to the black box in the left-hand panels.

AR-associated air parcels lose their moisture content when advecting over colder ocean surfaces and isentropically ascend.

As shown by Figure 4c, the DU p-AAR is detected over the cloud-free region adjacent to the AR. One possible explanation for this is that the extent of the DU p-AAR is initially the same as the AR, but the DU aerosols present in the AR are scavenged in- or below-cloud along the way. This would lower their atmospheric concentration and hence the poleward flux, which would no longer be detected as a p-AAR. This hypothesis is consistent with the vertical profiles during the event (Figure A2): DU is mostly found in large quantities where no liquid/ice water is found, and over the region of lower precipitation along the transect, but the mixing ratio is very low wherever water, including precipitation, is found. Figure A2 also shows, similar to the previous cases, that the transport of aerosols takes place at higher altitude than moisture transport.

In summary, these case studies show that (a) the p-AAR detection algorithm reproduces well important aerosol transport events, (b) aerosols and moisture during combined AR/p-AAR events are not transported at the same altitudes, and (c) aerosols and moisture do not necessarily follow the same large-scale pathways nor originate from the same area, even though they impact the same receptor region.

3.3. Characteristics of p-AARs

In this section we present the climatology (1980–2022) of p-AARs (i.e., poleward p-AARs that reach high latitude areas) and show their similarity and differences compared to ARs, including the impacted areas and seasonality.

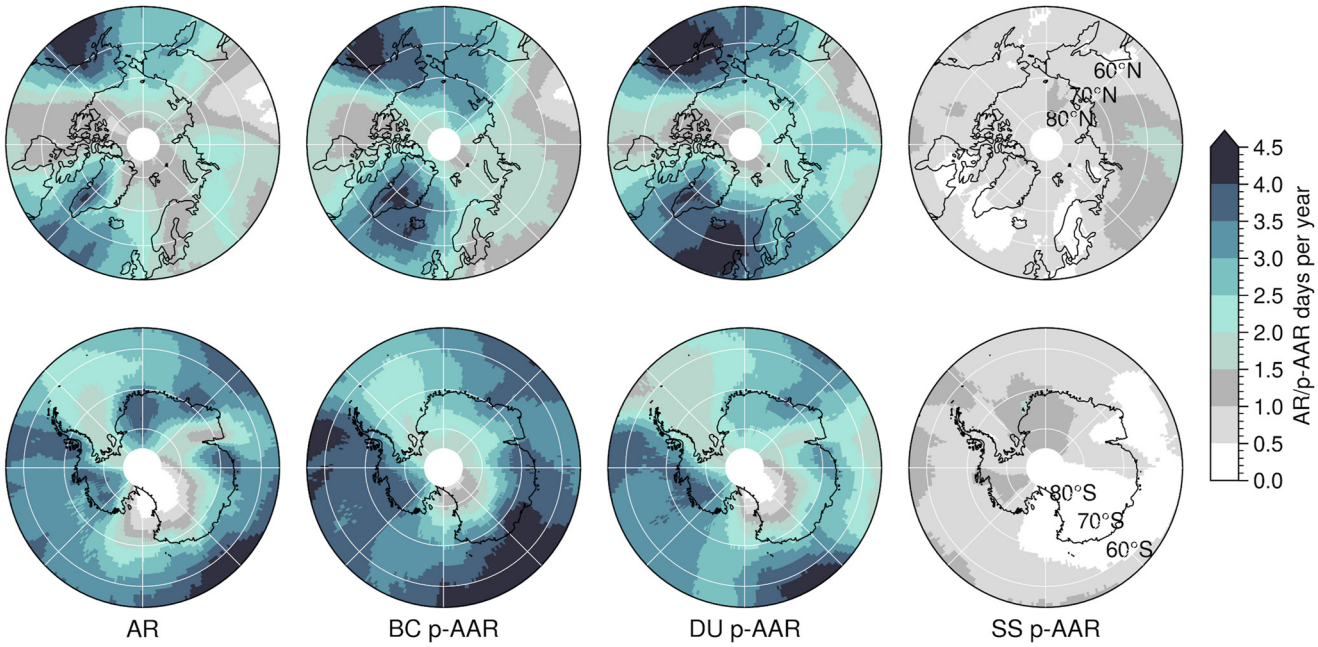

Figure 5. Climatology of polar Atmospheric Rivers and polar Aerosol Atmospheric Rivers. Frequency of Atmospheric River (AR - left), Black carbon (BC - middle-left), Dust (DU - middle-right) and Sea salt (SS - right) polar Aerosol Atmospheric River (p-AAR) detection, expressed as a number of days per year under AR/p-AAR for each grid point. This climatology covers the period 1980–2022.

We also explore the trends in the frequency of occurrence of p-AARs and ARs between 1980 and 2022 for the Arctic and Antarctic.

3.3.1. Climatology

We present a high latitude poleward p-AAR climatology and investigate the regions most affected by p-AAR events and the seasons of stronger activity, in order to establish a comparison with ARs. In the Arctic, BC p-AARs are mostly detected in the northern Atlantic, reaching the Greenland and Iceland regions, and in the northeastern Pacific, reaching Alaska predominantly, and the Bering strait area, with a frequency of up to 5 days per year for the 1980–2022 period (Figure 5). To some extent, DU p-AARs are found in the same regions as BC p-AARs, except for an eastward displacement in the Atlantic where higher frequencies are obtained, and an additional pathway over Russia that does not appear in BC p-AARs. Overall, DU p-AARs are also more frequent than BC p-AARs. Since sources of SS are more evenly distributed around the globe and closer to the polar regions compared to BC and DU, SS p-AARs are much less frequent, with a maximum frequency of 2 days per year. They also present a unique spatial distribution: The maximum of SS p-AAR detection frequency and dominant pathway is located in Russia, far from significant SS sources, where baseline concentrations are very low but fast transport can occur. Although these SS p-AARs do not seem to reach the high Arctic, this is an interesting feature showing how different aerosols can trace different pathways. This feature can also be related to a known issue of errant sea spray emissions over the Caspian and Black Seas in MERRA-2 (Randles et al., 2017). Elsewhere, the detection frequency of SS p-AARs is more homogeneous and generally less than 1 day per year. Compared to ARs, BC and DU p-AARs have similar frequencies of occurrence and spatial distributions overall, except at higher latitudes, where p-AARs can be two times more frequent than ARs, for instance in northern Greenland and the central Arctic.

In the Antarctic, BC p-AARs are more frequent than DU p-AARs, in contrast to the Arctic. p-AARs generally affect similar areas as ARs, except for Queen Maud Land (20°W–45°E), which is frequently reached by ARs, but seldom affected by p-AARs. The finding for the Arctic that p-AARs are more frequent than ARs at higher latitude does not apply for the Antarctic. SS p-AARs are less frequent than BC and DU p-AARs in the Antarctic too, and predominantly reach the Weddell Sea and Coats Land region (36°W–20°W). An important difference between p-AARs in the Arctic and the Antarctic is that, in the Antarctic, p-AARs (and ARs likewise) tend to be able to reach higher latitudes more frequently. While the frequency of AR/p-AAR crossing 80°N is less than 2.5 days per

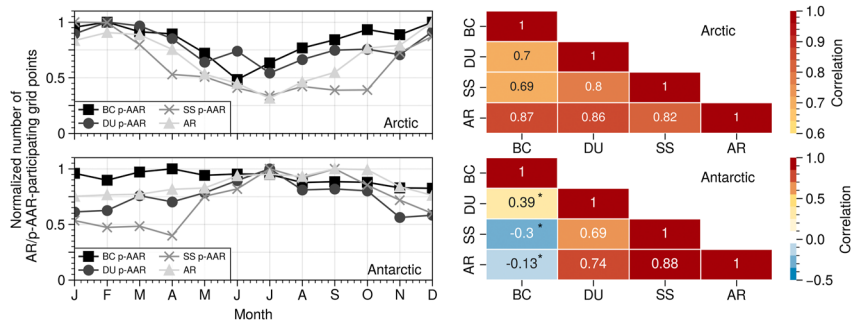

Figure 6. Seasonality of polar Atmospheric Rivers and polar Aerosol Atmospheric Rivers. Normalized monthly average frequency of polar Atmospheric Rivers (AR) and polar Aerosol Atmospheric Rivers (p-AAR) grid points (left) for the Arctic (65°–85°N - top) and the Antarctic (65°–85°S - bottom) and correlation matrix between these seasonal cycles (right). Period 1980–2022. Stars in the matrix indicate non-significant Pearson correlation coefficients at the 95% level.

year in the Arctic, they can penetrate as far as 85°S in West Antarctica with twice the frequency. This suggests a possibly larger impact (through change in, e.g., clouds, precipitation, albedo) of ARs/p-AARs on the Antarctic ice sheet than on the central Arctic sea ice, because of the stronger polar vortex around Antarctica which generally limits intrusions of lower-latitude air masses.

In the Arctic, averaged at the regional scale (65°–85°N), the seasonality of p-AARs (analyzed using the number of p-AAR points per month) is similar to that of ARs, with maximum frequency in winter months and minimum activity in summer months, and a correlation of at least 0.69 among these four types of AR/p-AAR (Figure 6). For ARs, this can be related to higher background levels of moisture in the summertime atmosphere (Rinke et al., 2019) which, due to the threshold definition criterion, causes fewer situations to be categorized as AR in this season, along with the position of the Arctic dome that does not favor long-range transport in summer, including of aerosols (Boyer et al., 2023). This makes the long-range transport relatively less important, as opposed to winter/spring when the polar dome is more expanded which facilitates long-range transport from lower latitudes (Boyer et al., 2023; Pernov et al., 2022). The DU p-AAR seasonality shown here is consistent with the seasonality of DU transport to the Arctic shown in Böö et al. (2023). SS p-AARs stand out, with a stronger seasonality and more rapid transitions between the winter and summer frequencies, resembling more a binary regime shift than a smooth seasonal evolution (cross markers in Figure 6). This latter cycle is harder to interpret as there are few SS p-AAR events per year (Figure 5), but it may be related to the seasonal cycle of sea ice cover: when sea ice is at its minimum extent, between late spring until late fall, more open ocean is present compared to winter, and therefore more SS is emitted locally. As a result of these local emissions, the background SS loads are higher than in winter, and the relative contribution of transport is thus less important, which is why SS p-AARs are less often detected.

In the Antarctic (65°–85°S), the seasonality is less clear, especially for BC p-AARs which do not feature a seasonal cycle and are, as a result, not correlated with the other three types of AR/p-AAR at the 95% level. This absence of correlation is interesting as it can signal a more steady occurrence of BC p-AARs throughout the year, which provides a more systematic and non-seasonally dependent way of analyzing extreme transport events. Here again, the seasonality of SS p-AARs is stronger than for the other species, also most likely related to sea ice cover seasonality like in the Arctic. Given how the sulfate content of SS in ice and firn, which varies with seasons, may be used to recover the seasonality of precipitation and reconstruct annual surface mass balance (Goursaud et al., 2019), coupling this feature with SS p-AAR detection can provide insight for the reconstruction of seasonal climate variations.

Despite their relatively low frequency of occurrence (generally less than 1% of the time - Figure 5), p-AARs account for a notable fraction of the total annual meridional transport of aerosols to the poles (up to more than 14%), as illustrated in Figure A3. The fraction of BC transport to the Arctic driven by p-AAR ranges from 3% around the North Pole up to 8% in the Bering Strait area and North Atlantic. Over the Southern Ocean, 8%–12% of BC transport occurs through p-AAR, down to around 5% in Antarctica. For DU, this fraction is even higher with more than 14% in Northern Europe and 12% over the Bering Strait area, and more than 10% in the Southern Ocean. Given the lower frequency of occurrence of SS p-AAR, their contribution to SS transport is also lower

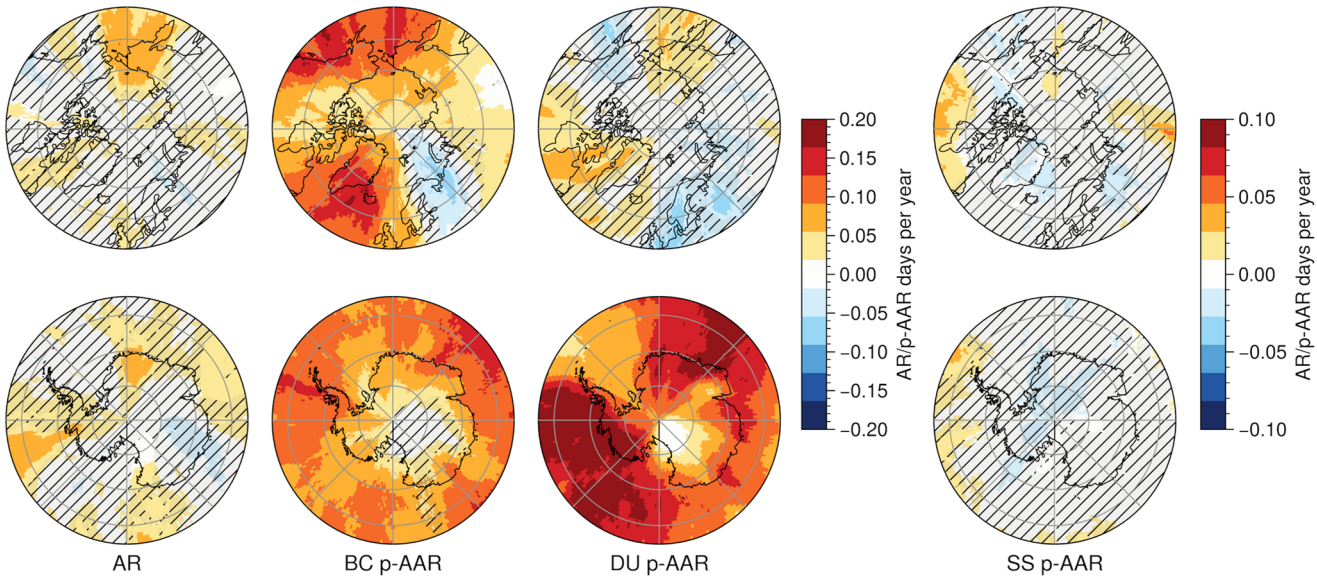

Figure 7. Trends in polar Atmospheric Rivers and polar Aerosol Atmospheric Rivers. 1980–2022 trends in Atmospheric Rivers (AR - left), Black carbon (BC - middle-left), Dust (DU - middle-right) and Sea salt (SS - right) polar Aerosol Atmospheric Rivers (p-AAR). Trend coefficients are computed as a linear regression of the time series of yearly AR/p-AAR over the period, for each grid point. Hatching indicates non-significant trends at the 95% level against a Mann-Kendall test.

than for BC and DU, with most values below 6% and rarely exceeding 8%. Contrary to BC and DU, this fraction for SS is generally larger over land than oceanic areas.

3.3.2. Trends

This section investigates the spatial and temporal trends of p-AARs, including a comparison with AR trends, in order to assess whether they similarly reflect changes in the climate. We explore whether there is a connection between the evolution in the frequency of AR/p-AAR events and the amount of the corresponding transported species present in the atmosphere. For aerosols, this amount is represented as the total annual emissions. For water vapor, we use annual mean surface atmospheric concentrations. AR/p-AAR are short-lived events and therefore are not directly linked to annual quantities of aerosol/water, but on long time scales the evolution of the latter quantities is representative of the availability of the transported tracers, and therefore connect to AR/p-AAR frequency.

If there is more moisture/aerosol available, even with no evolution in transport patterns, more AR/p-AAR will be detected since the historical threshold will be crossed more frequently. In a warming climate, due to the Clausius-Clapeyron relationship, the water content in the atmosphere increases and therefore more AR should be detected. As a result of this correlation, it is hard to disentangle the effect on AR frequency of the warming climate and of changes in circulation patterns. Primary aerosol emissions on the other hand are not as strongly affected by the warming climate, which may be an opportunity to isolate the change in extreme poleward transport frequency using p-AAR. This idea is explored in the next paragraphs.

Figures 7 and 8 show that ARs feature significantly (at the 95% level) increasing trends at the regional level since the 1980s, despite spatial heterogeneity, with similar magnitudes at both poles. The underlying causes for these trends remain an open question (Wille et al., 2019, 2022). Increasing amount of water vapor in the atmosphere at the mid-latitudes as the climate warms could partly explain this (Gershunov et al., 2017). For the Arctic, changes in circulation, with increasing frequency of blockings also drive the increase in moisture transport (Nygård et al., 2020; You et al., 2022), whereas in Antarctica, trends on the Amundsen Sea Low might explain AR trends in the Amundsen-Bellinghausen Sea (Turner et al., 2013; Wille et al., 2021). Trends in AR activity across Antarctica are similar with previously observed trends, but are slightly sensitive to the choice of the reanalysis product used for AR detection (Wille et al., 2021). Figure 8 illustrates that, overall at the hemispheric level, the evolution of high latitude poleward ARs is closely correlated with the evolution of hemispheric averages of water vapor mixing ratio at 1000 hPa. p-AARs on the other hand display a variety of trends depending on the pole and species considered (Figure 7).

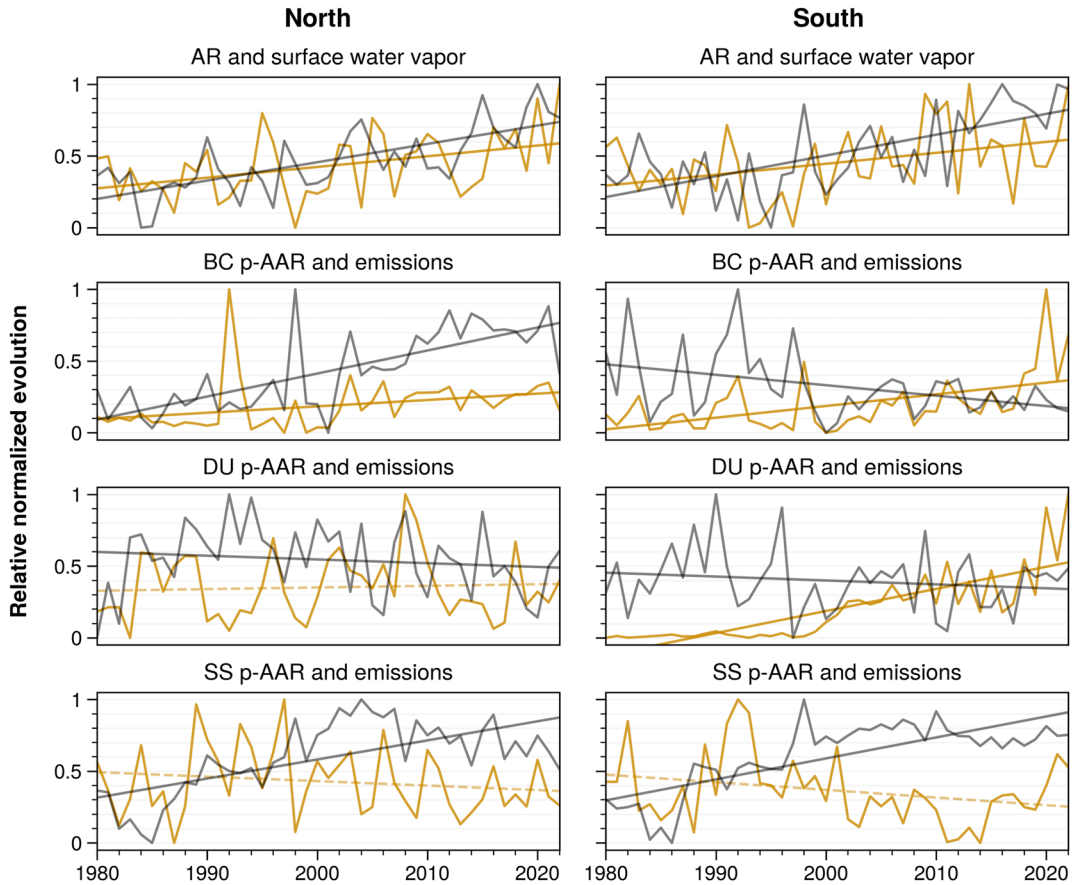

Figure 8. Evolution of polar Atmospheric Rivers and polar Aerosol Atmospheric Rivers. Time series of the annual number (yellow line) of polar Atmospheric Rivers (AR) and polar Aerosol Atmospheric Rivers (p-AAR) in the Arctic (65°–85°N - left) and Antarctic (65°–85°S - right), and evolution of annual emissions of aerosols (1000 hPa water vapor mixing ratio for AR) in the northern (0°–90°N) and southern (0°–90°S) hemisphere (black line). Straight lines indicate linear regressions (solid lines if the trend is significant at the 95% level based on a Mann-Kendall test, dashed line otherwise). All time series are normalized to vary between 0 and 1 in order to compare the relative trends. Period 1980–2022. NB: emission trends remain similar if the cut-off is performed at 30° latitude instead of the equator (see Figure A5).

BC p-AARs tend to generally increase over time in the Arctic, except over the Finland/Russia corridor where a significant decreasing trend is observed (Figure 7). BC p-AARs strongly increase in the North Atlantic, while BC emissions decrease in Europe and do not display trends in North America (Figure A4). This suggests that the evolution of North Atlantic p-AARs may be driven more by changes in circulation than changes in source intensity. However, BC p-AARs are also strongly increasing in the Bering Strait area, which is more directly under the influence of aerosol transport from the Indo-Gangetic plain and East Asia (Backman et al., 2021; Ikeda et al., 2017; Zhao et al., 2022). Figure A4 shows that BC emissions in Asia have been increasing over the period. The resulting increase in BC p-AAR frequency over the Bering Strait may thus be connected to the change in source activity and not only changes in dynamics, contrary to the North Atlantic sector. In the Antarctic, BC p-AARs are more homogeneously increasing, with only a portion of East Antarctica not showing a significant trend. In parallel, BC emissions decrease in the Amazon region in MERRA-2 (Figure A4), which drives the hemisphere-averaged decrease, but strong increases in emissions are found in southern Africa and south Asia. The resulting increasing trend in BC p-AARs suggests that either (i) African and Asian BC sources are more important than South American sources for Antarctic-reaching BC p-AARs, or (ii) changes in circulation dominate the evolution. Note that averaging emissions only below 30°S/above 30°N instead of the whole hemisphere, results in the same conclusions (Figure A5).

DU p-AARs do not feature significant trends in the Arctic on average (Figure 8), due to slight increases in Northeast America and Siberia compensated by slight decreases over Europe and Alaska (Figure 7). At the same time,

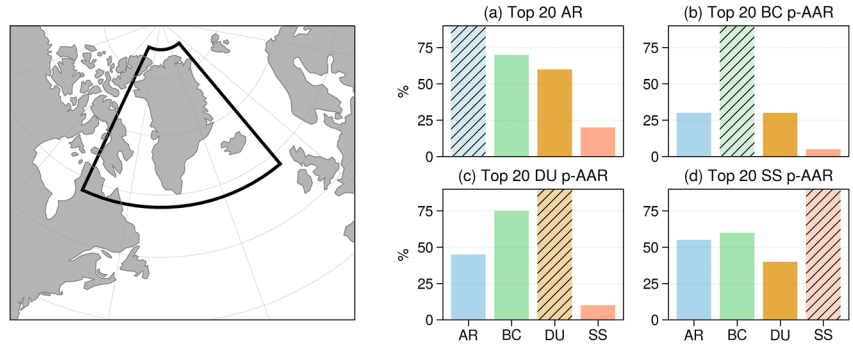

Figure 9. Top 20 polar Atmospheric Rivers and polar Aerosol Atmospheric Rivers in Greenland. Blue bars are Atmospheric Rivers (AR), green bars are Black carbon (BC) polar Aerosol Atmospheric Rivers (p-AAR), yellow bars are Dust (DU) p-AAR, red bars are Sea salt (SS) p-AAR. (a) Composite of the top 20 ARs in terms of cumulated meridional Integrated Vapor Transport (v*IVT*) reaching Greenland, and associated p-AARs. Panel (b) same as (a) but for the top 20 BC p-AAR. Panel (c) same as (b) but for DU p-AAR. Panel (d) same as (b) but for SS p-AAR. The area considered for compositing is the black box in the left panel. The percentage corresponds to the fraction of days for which other AR/p-AAR types are detected at the same time as the top AR/p-AAR.

emissions are slightly decreasing in the northern hemisphere (Figure 8). For the Antarctic, a strong increasing trend is observed everywhere (Figure 7), despite a slight decrease in emissions (Figure 8). However, the decrease in emissions hides an important heterogeneity: while DU emissions decrease in Australia over the period, they increase in Patagonia at the same time (Figure A4). The fact that the resulting DU p-AAR trend has on average a strong increase (Figure 8) suggests that the South American DU sources are generally more important than Australian sources for Antarctic DU p-AARs. This is consistent with the usual dominant transport pathways of DU to Antarctica (Neff & Bertler, 2015), but differ from the finding by Li et al. (2008) that sources in South America and Australia contribute equally to the average DU transport to the Antarctic.

SS emissions have been increasing globally over the course of the 20th century (Figure A4), driven by increases in wind speed and decline of sea-ice cover (Lapere et al., 2023). As a result of the increasing emissions, the historical threshold is more and more likely to be exceeded, and therefore an increase in SS p-AAR would be expected over the last decades under unchanged transport dynamics. However, contrary to this expectation, the corresponding trend in SS p-AARs is on average non-significant (Figure 8) and even slightly decreasing at higher latitudes, particularly over Greenland and Antarctica (Figure 7). This might suggest that the dynamical mechanisms generating SS p-AARs have been generally weakening over the last 40 years.

In summary, current trends in p-AAR (a) are different from trends in AR, (b) are diverse depending on the type of p-AAR (BC, DU, SS), (c) have clear differences between the poles, and (d) are not clearly correlated with emission trends. All of the above suggests that AR and p-AAR detections have the potential to be complementary tools that can be used together for a number of applications, as will be further discussed in Section 4.

3.4. Co-Occurrence of Strongest p-AARs and ARs

This section investigates the strongest AR/p-AAR of each type that reached Greenland and the AP, between 1980 and 2022. These two regions are often studied in the AR literature, hence their choice as receptor regions here. The top AR and p-AAR days are ranked based on the cumulated v*IxT* within an AR/p-AAR event detected inside the black contours in the left panels in Figures 9 and 10. The top 20 of these events are then analyzed as a composite, and their co-occurrence with other types of AR/p-AAR is quantified.

For Greenland, the 20 strongest ARs are frequently associated with BC p-AARs (70% of events), around 60% of the time with DU p-AARs, and less than 20% with SS p-AARs (Figure 9a). These top AR events originate from the northwest Atlantic Ocean (Figure A6). In contrast, the strongest BC p-AARs affect primarily eastern Greenland, coming from the northeastern Atlantic Ocean or continental North America (Figure A6), and occur mostly independently from the other types of AR/p-AAR, with co-occurrences in less than 30% of the cases (Figure 9b). Major DU p-AARs originate either from the continental North America or from Northern Africa, where important dust sources exist, and are associated with BC p-AARs for up to 75% of cases (Figure 9c). ARs are present

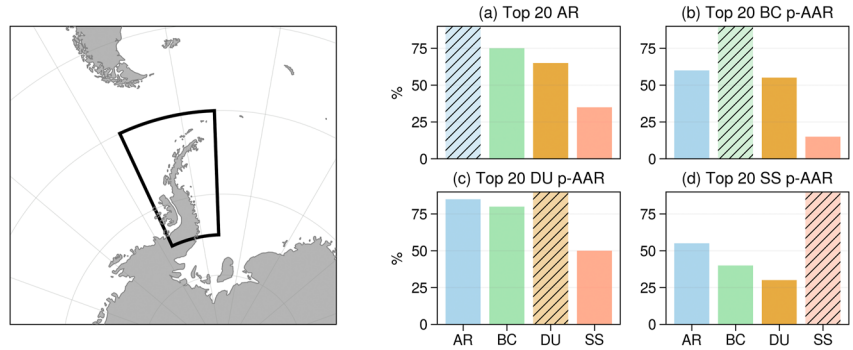

Figure 10. Top 20 polar Atmospheric Rivers and polar Aerosol Atmospheric Rivers in the Antarctic Peninsula. Same as Figure 9 but for AR/p-AAR reaching the Antarctic Peninsula (AP).

for 45% of the top DU p-AARs, and SS p-AARs are mostly absent. Finally, major SS p-AARs are often associated with ARs and BC p-AARs (more than 50%), and with DU p-AARs only in 40% of cases (Figure 9d). Generally, major ARs tend to be associated with p-AARs, but the opposite is not the case. p-AARs can occur within relatively dry air masses not classified as ARs.

In the AP, the co-occurrence of all types of AR/p-AAR is generally more frequent than in Greenland (Figures 10 and A7). Top SS p-AARs feature less frequent co-occurrences than the other types of AR/p-AAR (Figure 10d). 75% of the top ARs are also BC p-AARs (Figure 10a), and more than 75% (50%, respectively) of the top DU (BC, respectively) p-AARs are associated with co-located ARs (Figures 10b and 10c). Another difference between Greenland and the AP is that the top AR/p-AAR for Greenland feature a variety of orientations and thereby source region, whereas in the AP all these events have a similar axis, with an origin near the tip of South America (Figure A7). Trajectories also appear to be more narrow for the AP than Greenland. This can be related to more distributed aerosol sources and more diverse transport pathways in the Arctic. Figure 10 also shows that the top ARs/p-AARs reaching the AP are more often coinciding with other types of ARs/p-AARs also reaching the AP than it is the case for Greenland (except for SS p-AAR). Although a more thorough investigation is required to explain this difference, this may suggest that in the AP, extreme AR/p-AAR events are driven more by the dynamics, since all the quantities are transported, whereas in Greenland those large events may be driven both by transport patterns and emission sources, due to the closer proximity of those sources.

4. Potential Applications of p-AARs

The general characteristics of p-AARs and the case studies presented above suggest that p-AARs can have relevance for several applications, interesting for both the aerosol and the climate communities. In the following we explore some of these potential applications.

4.1. On the Co-Occurrence of p-AARs and ARs

The association between ARs and p-AARs could be used to understand both how aerosols modify cloud properties and for understanding aerosol wet deposition. BC and DU aerosols are important species when it comes to liquid and mixed-phase clouds, as BC can act as CCN (Quinn et al., 2011; Zieger et al., 2023) and DU can act as INP (Irish et al., 2019; Kawai et al., 2023; Yun et al., 2022). Therefore, when ARs and p-AARs are combined, cloud properties could be different compared to AR-only cases, with impacts on cloud albedo and/or precipitation timing. Also, since ARs are important contributors to precipitation in the AP (Maclennan et al., 2023; Wille et al., 2021), ARs that are also p-AARs could scavenge (wet removal in and below clouds) the high aerosol content, resulting in deposition to the ice sheet upon precipitation, which can darken snow and ice surfaces, and trigger the ice albedo feedback (Bond et al., 2013; Skiles et al., 2018). The co-localized presence of large amounts of moisture and aerosols can also significantly increase aerosol optical depth through the uptake of water by hygroscopic aerosols, with direct impacts on surface radiation.

These possible impacts are illustrated by the difference in total column and atmospheric surface mass concentration of aerosols, as well as aerosol optical thickness (AOT), during the top 20 combined AR/p-AAR events

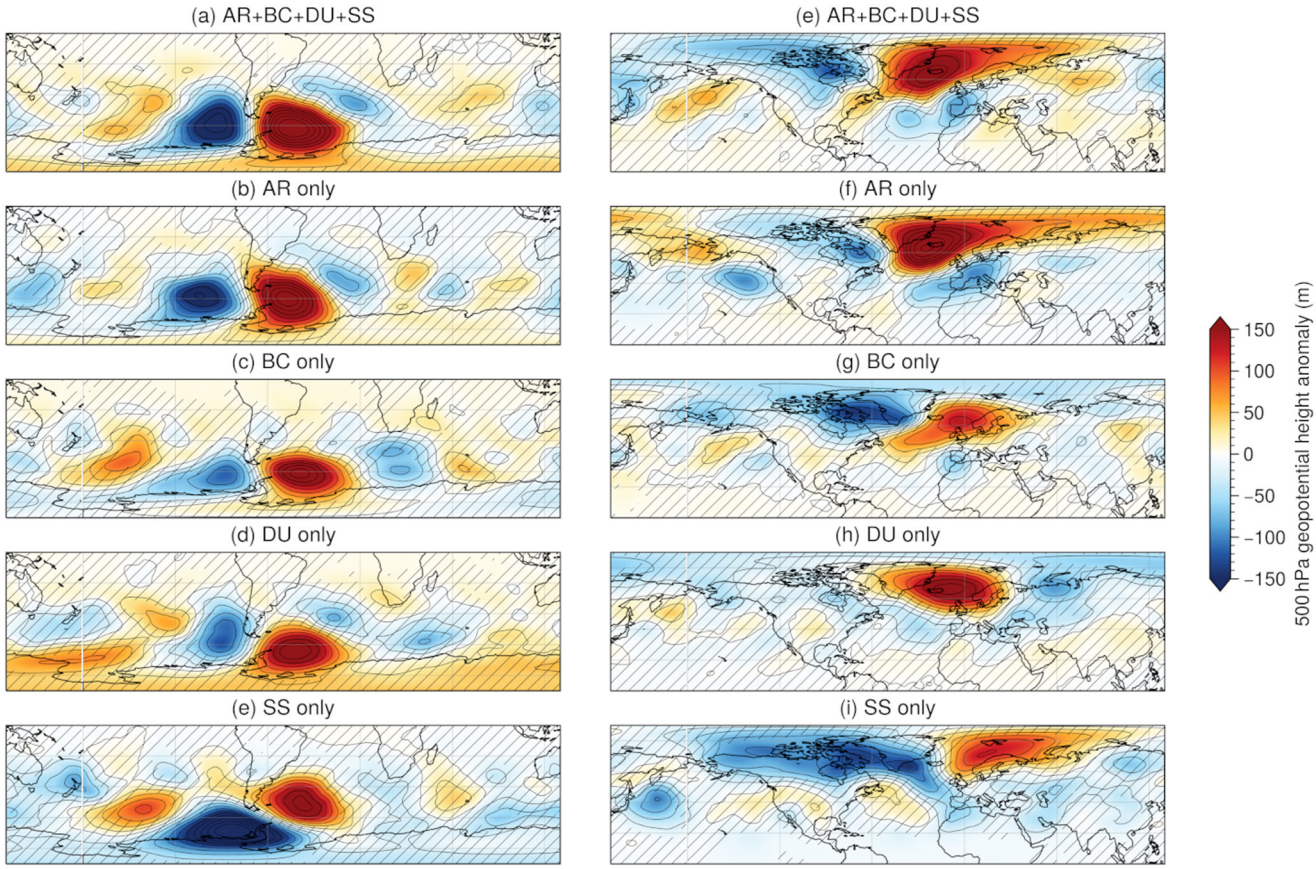

Figure 11. Geopotential height anomalies during top events. Composite of 500 hPa geopotential height anomalies for the top 20 events of 5 different types reaching the Antarctic Peninsula (left) and Greenland (right). (a, e) Co-occurring Atmospheric River (AR) and polar Aerosol Atmospheric River (p-AAR) of all aerosols. (b, f) AR only with no p-AAR. (c, g) Black carbon (BC) p-AAR only. (d, h) Dust (DU) p-AAR only. (e, i) Sea salt (SS) p-AAR only. Geopotential height from MERRA-2. Hatching indicates areas where the standard deviation of the anomaly among the events is two times larger than the absolute value of the average anomaly.

(i.e., simultaneous detection of AR, BC p-AAR, DU p-AAR and SS p-AAR) compared to the top 20 AR events without associated p-AAR in Greenland (Figure A8) and the AP (Figure A9). These top 20 AR/p-AAR are ranked based on the daily mean v*IVT* averaged over the region defined by the black contours in Figures A8 and A9.

Over Greenland, atmospheric surface mass concentration of BC and DU increase by up to 15 ng m^{-3} and 1 μg m^{-3}, respectively, when AR and p-AARs occur simultaneously compared to AR-only cases (Figure A8a), indicating that transport does not only occur at high altitudes in the atmosphere. SS surface concentrations mostly increase over the ocean but the anomaly can reach up to 3 μg m^{-3} over Greenland. For all aerosols, the total column mass density also has a positive anomaly during AR + p-AAR events (Figure A8b). Similarly, AOT increases by up to 0.08 in the Greenland region (Figure A8c). The largest increases in AOT are correlated with the largest increases in SS mass. Given the highly hygroscopic nature of SS, the combined presence of high moisture levels through the AR, and SS through the SS p-AAR, explains this large increase in AOT, which can have major impacts on the radiative balance through the aerosol-radiation interaction. For the AP, similar conclusions can be drawn as for Greenland, except for DU for which the surface transport contributes more to the total column compared to Greenland (similar change in total column, but surface concentrations 10 times larger). Based on Figures A8 and A9, it is important to distinguish between clean and polluted ARs for understanding precipitation, albedo, radiation and melting impact of ARs. p-AAR detection provides a way to do so, and facilitates conducting more holistic impact studies.

The synoptic conditions are different when AR and p-AAR occur simultaneously compared to cases when each type of AR/p-AAR occurs independently, as shown in Figure 11. For Greenland, there is a larger diversity of synoptic situations for the top 20 AR/p-AAR compared to the AP. The geopotential height anomalies are similar for combined AR/p-AAR (Figure 11e) and AR-only (Figure 11f) cases, with a strong high centered on Iceland, and

a comparatively weaker low above eastern Canada. The cases where only BC p-AARs are detected are associated with similar spatial patterns but the low is comparatively stronger, and the high comparatively weaker, in addition to a slight eastward displacement which connects Greenland with North American air masses (Figure 11g). For DU p-AAR days, the transport is driven by a strong high located over the Norway sea, enabling transport from North Africa but without an associated low pressure system (Figure 11h). In other words, the transport in this case is probably slower, but more sustained and with less wet scavenging. SS p-AAR cases exhibit, for Greenland as well, circulation patterns different from all the others: a large area of low pressure covering Canada and extending until Europe, and a weaker high near Svalbard (Figure 11i). This synoptic situation leading to local storms can export large amounts of open-ocean-sourced sea spray. As a result, SS p-AAR may not be as fit as BC and DU p-AAR for the purpose of characterizing long-range transport from the mid-latitudes.

In the AP, when all types of AR/p-AAR occur simultaneously, a strong high-low dipole with a longitudinal axis appears (Figure 11a), indicating that air masses originate primarily from continental South America. The situation is similar when ARs with no p-AAR occur, with the exception of the dipole axis which is tilted and therefore suggests air masses come from the southeastern Pacific Ocean rather than continental areas (Figure 11b). When only BC p-AARs are detected, the dipole is weaker, with a reduced intensity of the low in particular, and shifted eastward (Figure 11c), but the typical wave train of high-lows coming from Australia appears more clearly than in the other cases. The composite during DU p-AARs (Figure 11d) is similar to BC p-AARs, except for the tilt of the dipole which shows the influence of Patagonian dust sources in this configuration. In the case of SS p-AARs only, the synoptic situation is different from all the others: a very strong low covers the whole AP, surrounded by a strong high in the southwestern Atlantic Ocean and another high at the Pacific and Southern Ocean demarcation. This situation translates the fact that SS sources are closer to Antarctica (sea spray from the Southern Ocean), compared to the other aerosols, and are thus transported by strong winds associated with local storms during extreme events.

The differences in synoptic circulation described above can partially be attributed to the season during which these top events occur. For Greenland, compound events are mostly found in SON–DJF, with the exception of SS p-AARs which are more frequent in DJF–MAM (Figure A10). This last feature can be connected to the sea ice cover at that season, which implies a more important contribution from long-range transport to Arctic concentrations of SS. Cases with only DU p-AAR and only SS p-AAR are similarly found predominantly in JJA–SON in the Antarctic. For both poles, the events transporting all quantities simultaneously (AR + BC + DU + SS) have the same seasonal distribution: 50% occur during wintertime, and another 30% during the fall. This finding suggests that winter-fall weather regimes are more favorable for the occurrence of more intense ARs/p-AARs reaching Greenland/AP, in addition to being conducive to a higher frequency of AR/p-AAR occurrence irrespective of their intensity on average at the poles (as indicated by Figure 6). This similarity in the seasonality of combined events can be leveraged for studying, for instance, the comparative evolution, between the two poles, of the seasonality of extreme transport, over longer time scales.

In summary, differences in synoptic circulation appear when considering the five different types of AR/p-AAR (AR, BC p-AAR, DU p-AAR, SS p-AAR, and all combined), leading to different source/receptor areas during the strongest events. Polar BC p-AAR, and DU p-AAR are also usually polar ARs and vice versa, which can have a combined impact broader than only affecting aerosols or moisture independently. Therefore, they deserve to be treated as compound events, not in isolation. Because of their different pathways, p-AARs can sometimes connect relatively dry transport events to their impacts (e.g., precipitation) when ARs are not detected. This analysis supports the idea that adopting a clustering analysis using the 5 types of AR/p-AAR discussed here should be explored in future work.

4.2. Dry Extreme Poleward Transport

p-AARs can provide insight for cases of fast poleward transport of relatively dry air masses, that we have demonstrated to be significantly different from AR in terms of the circulation pattern (see Figure 11). In recent literature (Pohl et al., 2021), AR analogs were analyzed, showing important differences with polar AR events. By leveraging the p-AAR detection built in this work, future research could try to address the question: what if these AR analogs are p-AARs? If so, because of the difference in moisture content and radiation/cloud feedback (due to aerosols), the (thermo)dynamics of these two types of events should be different, despite leading to the analogous situations shown in Figure 11. The compared vertical structures of moisture/aerosol extreme transport

events, in particular, could help better describe the underlying physical processes. Adopting a new clustering method accounting for ARs, analogs and p-AARs instead of the first two only could pave the way toward a better understanding of the factors contributing to AR-like dynamics, and could help to explain the occurrence of non AR-related extreme temperature events (Wille et al., 2022).

4.3. Analyzing Future Poleward Transport Occurrences

Analyzing future AR frequency and intensity is complex. As the climate warms, more moisture is available, which constitutes a trend in the source of AR-carried water vapor (Gershunov et al., 2017), as shown in Figure 8. This trend makes it hard to untangle changes in circulation from changes in atmospheric water vapor content when exploring current and future trends in ARs (Bintanja et al., 2020; Rinke et al., 2019). In addition, the AR response to future climate change is highly dependent on the chosen detection tool (O'Brien et al., 2022; Shields et al., 2023). For natural aerosols, the emission sources are not expected to feature strong trends in future scenarios, although more sea salt (Lapere et al., 2023) and possibly slightly more dust (Zhou et al., 2023) can be expected under a changing climate. Local sources of anthropogenic aerosols such as BC are also expected to change moderately, particularly in the Arctic with increased shipping traffic (Corbett et al., 2010). However, the aerosol trends are less directly connected to the warming temperatures compared to the changes in moisture transport (Held & Soden, 2006).

p-AARs can offer robust and key information on the dependence of intrusions and ARs on climate change. The implementation of specific simulations, with controlled aerosol emissions, would make it possible to assess the future evolution of atmospheric intrusions considering only variations in atmospheric dynamics. The assessment of the future evolution of the frequency and intensity of ARs could then be treated by eliminating the increase in frequency of occurrence resulting directly from the Clausius-Clapeyron process. Another method could consist of introducing idealized aerosols with different residence times, or other tracers, in a general circulation model (Krinner & Genthon, 2003) and then to analyze the resulting p-AARs. Applying this approach based on tracer age for different climates would allow to analyze the climatologies of poleward transport, including in future climate.

4.4. Ice Core Analysis of Past AR Activity

The reconstruction of AR variations in past climate has been proposed through the analysis of water isotopes in ice cores, using the δO^{18} ratio (Servettaz et al., 2023), which can be related to changes in local temperature over long time scales (Jouzel et al., 1997). However, the use of the δO^{18}-temperature relationship in ice cores is complex, as it is related to changes in air mass origins, transport, sublimation of hydrometeors, post-depositional effects as well as diffusion in the firn (Buizert et al., 2014; Casado et al., 2018; Cauquoin et al., 2019; Krinner & Werner, 2003; Werner et al., 2001). Moreover, a direct relationship between δO^{18} or d-excess anomalies and temperature is not systematic (Wahl et al., 2022) and is insufficient to retrieve AR occurrence using this proxy alone. Aerosol analysis, through p-AARs, could complement water isotopes to retrieve past occurrences of extreme transport events, using a combined δO^{18}-aerosol analysis, since changes in aerosol content in ice cores could result from changes in meteorology (Levine et al., 2014; Rhodes et al., 2018). This connection can also be made for longer time scales, including paleoclimate reconstruction (Wolff et al., 2006).

In addition, Earth System Models (ESM) sometimes use aerosol content measured in ice cores for evaluating the simulated aerosol concentrations in past conditions (Moseid et al., 2022). However, it is not clear how well ESMs reproduce specific extreme events which can generate p-AARs, or more generally AARs (e.g., extreme boreal fires). These events can account for an important fraction of the aerosols deposited onto snow (J. L. Thomas et al., 2017) and found in ice cores. An evaluation of both AAR and p-AAR occurrences in ESMs could therefore help better understand the model limitations when comparing aerosol trends in ESM and ice cores, and provide insight into deposition of light absorbing particles onto the ice sheet.

4.5. Understanding Aerosol-Climate Interactions in Polar Regions

Aerosols influence both the formation and evolution processes within clouds, acting as CCN or INP. The latter, because of their scarceness and the predominance of ice and mixed-phase clouds in the Arctic and over Antarctica (Matus & L'Ecuyer, 2017), condition the cloud radiative effect and therefore the energy budget of these regions,

making them critical for understanding and predicting the polar climate (Murray et al., 2021). The systematic identification of ARs and p-AARs could be central in helping elucidate the predominant CCN and INP sources originating from rapid transport to the poles. Aerosol-cloud interactions within ARs have yet to be studied in detail. Depending on the meteorological conditions and the aerosol content and type within ARs, the cloud properties can be affected, as well as the precipitation timing which can be either accelerated or delayed. Conversely, aerosols can be washed away by intense precipitation during an AR, as was shown here for the February 2002 AR event in the AP. Comparing combined AR/p-AAR events with AR-only events could be an efficient way to quantify these interactions.

In addition to affecting clouds and precipitation, aerosols can darken snow and ice surfaces upon deposition and lower their albedo, triggering the ice albedo feedback (Bond et al., 2013; Skiles et al., 2018). Non-polluted ARs or combined AR + p-AAR likely have different impacts on the polar ice sheet, which deserves closer investigation, particularly in connection with the observed polar amplification in which ARs and aerosols could play an important role (Wendisch et al., 2023; Zhang et al., 2023).

Finally, the study of transport events of aerosols to the high latitudes usually relies on their detection from satellite or from field campaigns. Satellite measurement of aerosols in polar regions is complex and therefore limited, for several reasons. First, sea ice is too bright a surface for sensors to accurately separate the contribution to back-scattering from the ground and from aerosols (Mei et al., 2013). Second, cloud cover is predominant throughout the year both in the Arctic and Antarctic (Eastman & Warren, 2010; Lachlan-Cope, 2010), which impedes the retrieval of valid aerosol data. Field campaigns and ground-based measurements are also more limited in these remote regions. As a result, some important aerosol transport pathways or major events can be missed. The systematic detection of p-AARs using reanalysis or models can help identify all important events more exhaustively, which is particularly important given the current attention for a better quantification of aerosol-cloud interactions in polar regions. For this, dedicated high-resolution climate modeling of the detected events can help to provide a better understanding.

4.6. Adapting AR Algorithms for Heat Transport

The p-AAR detection developed here shows that the concept of AR detection can be extended to transported quantities other than water vapor. Another quantity of interest could be heat (Komatsu et al., 2018). The increased meridional latent heat transport (LHT) through ARs was shown for the mid-latitudes, in connection with the moisture transport, but the effect on sensible heat transport (SHT) is less clear (Shields et al., 2019). However, Shields et al. (2019) also show that under climate change scenarios, the increase in the 300 hPa meridional wind speed is a stronger driver of the increase in AR-related SHT than the 850 hPa meridional wind speed. This transport in the upper troposphere is also characteristic of the aerosol transport in p-AARs as shown in the different case studies in this work. The aerosol transport occurring higher up also connects to the findings from Papritz et al. (2022), who found that air subsiding from the mid-troposphere into the boundary layer is as important an airstream as surface fluxes for the transport of moisture to the Arctic in wintertime. Using similar algorithms for heat transport as developed for ARs and p-AARs, and cross comparing ARs, p-AARs and heat transport events could allow the community to understand how moisture, aerosols, clouds, latent heat release and heat advection interact during these events, and quantify how these interactions impact the heat budget at high latitudes.

4.7. Limitations

Future work building on the possibilities offered by p-AAR detection should however be careful to keep in mind that p-AARs have limitations, both from the point of view of their capability and their interpretation.

4.7.1. Aerosol Sources

Because aerosol sources over the globe are generally more localized than moisture, when analyzing specific regions of the Arctic or Antarctic, there is a risk of over-sampling certain trajectories that connect source and receptor regions. For example, when studying the AP, trajectories associated with Patagonian dust events could be over-represented due to the short distance and high activity of this source. This is particularly true for the Arctic where aerosol sources of all types are generally closer than in the Antarctic, which leads to transport events

occurring more frequently. As a result, extreme transport events described by p-AARs have a comparatively smaller importance when it comes to the annual aerosol budget in the Arctic than in Antarctica.

However, this possible sampling bias does not seem to appear in the climatologies presented in this work as both ARs and p-AARs feature similarities in spatial distribution and frequencies, despite different source regions (moisture mostly comes from the ocean, whereas BC and DU are mostly emitted from land). In this respect, one could argue that, perhaps, p-AARs are a signal of extreme transport of the global background aerosol, rather than a source-receptor connection. In that case, for example, a DU p-AAR in the Antarctic would not necessarily describe the transport of Patagonian or Australian DU, but extreme transport of air masses not coming from DU source regions, which carry background DU levels throughout the troposphere. This does not appear to be what happens in the case studies presented in Sections 3.2.1 and 3.2.2 where concentrations are much higher than background, but this could partly explain the lack of correlation, on average, between emission trends and trends in p-AAR that we show in this work.

4.7.2. Sea Salt Aerosol

Among the different aerosol types considered here, SS p-AARs seem to be a less adapted tool when it comes to the potential applications of p-AARs. First, because sources are more widespread and closer to the poles, particularly in the Southern Ocean, SS p-AARs are quite rare and seem to relate more to local large storms, rather than extreme transport of mid-latitude air masses. Furthermore, simulations show that the interpretation of sodium variability in Arctic ice cores can be either related to sea ice changes or meteorological factors, and depends on the area where the ice cores are drilled (Rhodes et al., 2018). As a result, the connection between sodium in ice cores and circulation patterns can be difficult to interpret. although at shorter time scales and for Antarctica, ice core sodium can be more directly related to meteorology (Levine et al., 2014). In comparison, BC and DU in ice cores might be more straightforward to relate to atmospheric processes as the sources are further away, and to some extent less seasonally dependent as they are not connected to sea ice cover variations.

Furthermore, SS can undergo re-suspension in sea ice and snow regions through the process of blowing snow (Frey et al., 2020; Yang et al., 2008). SS aerosols that were deposited onto coastal regions can thereby be transported further inland and eventually end up in non-coastal ice cores. As a result, SS aerosols that may have been brought to the poles through SS p-AARs can be transported several days later and several hundred kilometers away from the p-AAR region. This can create a bias in the connection between ice core sodium and p-AARs.

4.7.3. Current State of Aerosol Modeling

The representation of the polar aerosol budget in models and reanalysis is still uncertain. Emissions, transport and deposition are diversely represented. In particular, DU and SS mass concentrations are usually overestimated at high latitudes, including in MERRA-2, and differ depending on the model/reanalysis considered (Böö et al., 2023; Lapere et al., 2023). Because we only evaluate extreme events here, defined based on a relative threshold, this should not be a problem for p-AAR detection, but for impact studies this may be a limitation.

Furthermore, aerosol-radiation and aerosol-cloud interactions are still challenging to represent in climate models and reanalysis. In particular, the effect of aerosol content in ARs and the role of p-AARs in triggering precipitation, designated above as a topic that can benefit from p-AAR detection, is not straightforward to estimate. The extent to which p-AARs exert a meteorological feedback, which could help self-sustain or dampen the transport, is also not possible to evaluate at this state of climate modeling, although this would be critical information for understanding the physical processes controlling extreme transport events. Similarly, even in the latest generation of models, transport and deposition (dry and wet) processes in polar regions are challenging to accurately model, which can affect both the quality of the p-AAR detection and the impact studies.

However, these aerosol-climate interactions are better represented in smaller scale models, such as regional chemistry-transport models (CTMs) and regional climate models (RCMs). We believe that using the AR/p-AAR catalogs can help identify test cases of interest which can then be simulated using high-resolution CTMs/RCMs. Evaluation and sensitivity analysis for these cases can help isolate and quantify the impact on clouds and precipitation, and eventually on cryosphere melting, of the aerosols present in p-AARs. Furthermore, deposition fluxes of BC and DU can be computed, and the impact on snow and ice albedo can be evaluated.

5. Conclusions and Perspectives

In this work, we create a polar-specific p-AAR catalog for BC, DU and SS aerosols, by leveraging and adapting an AR detection algorithm. We validate the p-AAR detection by analyzing case studies and comparing with AR climatologies, including evaluating the sensitivity of detection to the threshold chosen. We present the climatology and seasonality of p-AARs, in the Arctic and Antarctic, and show that they are often similar to ARs, but also have different characteristics that have added-value for understanding poleward transport processes. We also present the trends in p-AARs over the last 40 years, which do not show a connection with the evolution of aerosol emissions. In comparison, AR trends are well correlated with the increase in atmospheric moisture.

The detailed study of three major AR and p-AAR events shows that they can originate from different remote source regions and eventually converge in a confluent manner resulting in similar trajectories just before landfall. These case studies also show that aerosols and moisture are not transported at the same altitudes. Overall, they indicate that a more holistic approach of extreme transport events is needed instead of moisture-only or aerosol-only analyses. Composites over the strongest AR/p-AAR of each type further illustrate the complementary nature between AR and p-AAR, as they are associated with different synoptic circulations. These composites also show that co-occurring AR and p-AAR bring large amounts of aerosols near the surface compared to AR events with no p-AAR.

The potential applications of p-AARs that should be explored in future work include:

1. Gaining a holistic understanding of rapid transport from the mid-latitudes to the poles. Because the dynamics involved in p-AAR and AR can be similar in some cases, but the sources, or zones of uptake and uplift of moisture differ from aerosols, combining both ARs and p-AARs can provide a more holistic understanding of the transport of mid-latitude air masses to the poles. This can aid in better understanding the underlying physical processes and their feedbacks, that are critically important for polar climate including, for example, cyclogenesis, blocking amplification, clouds, and precipitation.
2. Understanding aerosols preserved in ice, firn, and snow. p-AAR detection is one tool that can be used to help understanding how aerosols arrive on the ice sheets and aid in interpreting chemical signals stored in polar ice, firn, and snow. p-AAR catalogs take into account changes in emissions, transport and wet or dry deposition, which is important for understanding what species are stored in the ice core record and how the associated air masses were transported from the mid-latitudes to the poles. The approach could also be extended for future climates, and to tracer age analyses based on controlled emissions of various tracers, giving information on transit times and pathways to the ice sheet.
3. Quantifying the impact of extreme aerosol transport on polar climate. Systematic studies of major aerosol intrusions through p-AAR can provide a way of quantifying both the aerosol direct (aerosol-radiation interactions) and indirect (aerosol-cloud interactions) effects, as influenced by transport from the mid-latitudes. Event detection and clustering can, for example, suggest p-AAR impacts on polar clouds and precipitation.

In summary, we provide a catalog of p-AARs that are a new and unique tool that can provide a better understanding of polar climate and its connections with the mid-latitudes.

Appendix A

A1. Supplementary Figures

Below are additional figures illustrating the case studies and statistical description of p-AARs (Figures A1–A10)

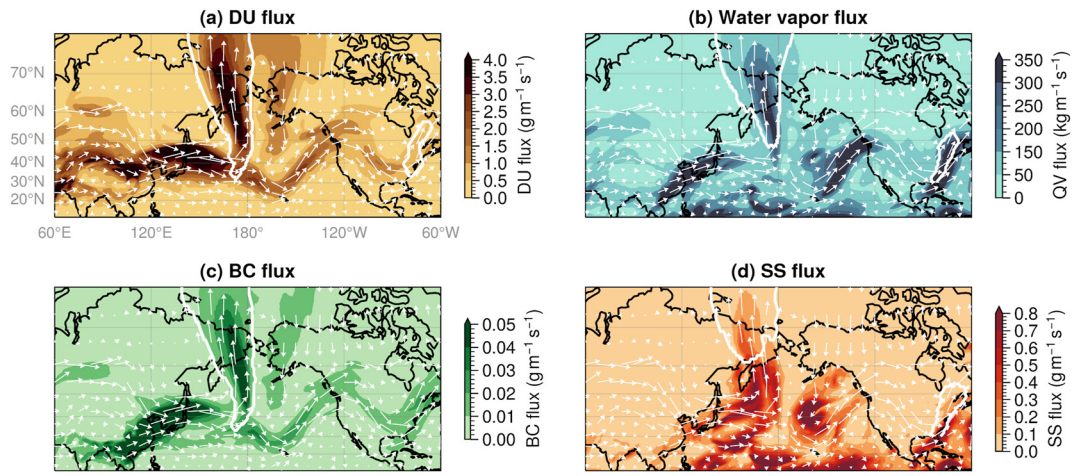

Figure A1. Fluxes on 2013-03-12. Vertically integrated Dust (DU) (a), water vapor (b), Black carbon (BC) (c) and Sea salt (SS) (d) flux (zonal and meridional) from MERRA-2 on 2013-03-12 (colormap) and associated 500 hPa wind field (arrows). White contours indicate Atmospheric River/polar Aerosol Atmospheric River detection for each species.

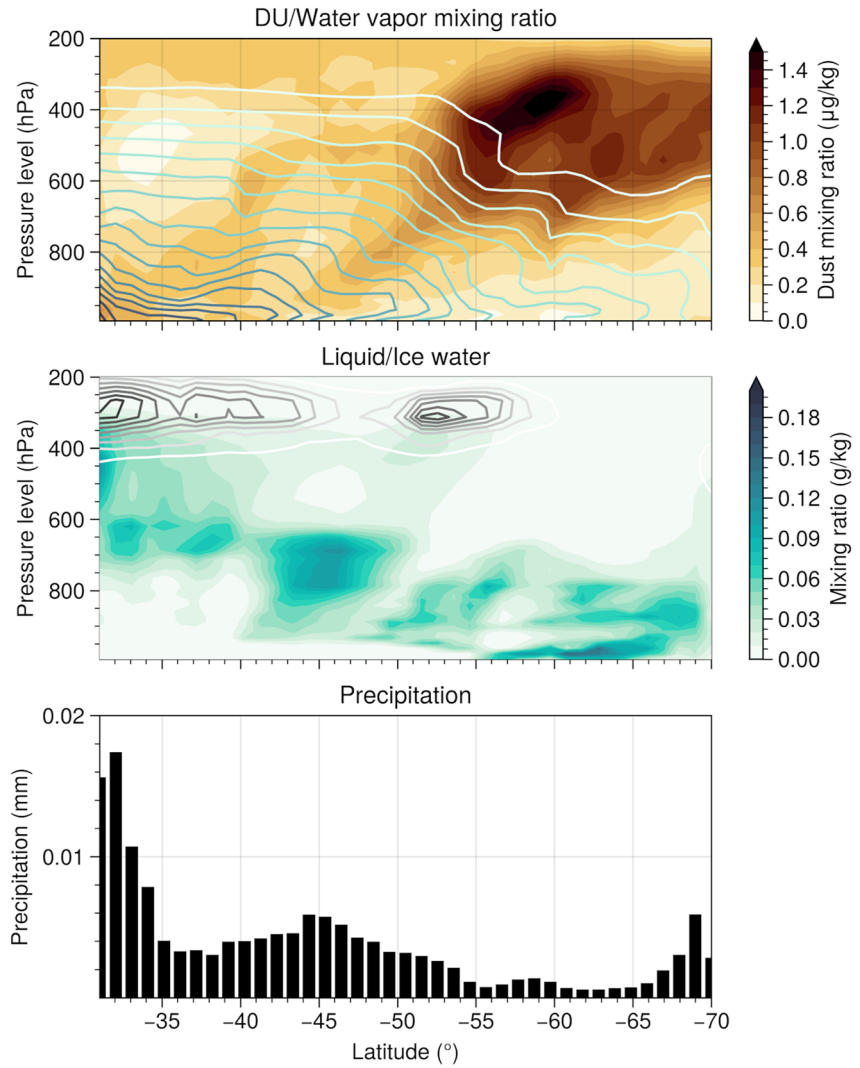

Figure A2. Vertical profiles during the 2002-02-19 Antarctic Peninsula case. Vertical profiles along the white transect in Figure 4c. Top: Dust (DU - colormap) and water vapor (contours) mixing ratio. Middle: Liquid (colormap) and ice (contours) water mixing ratio. Bottom: surface precipitation.

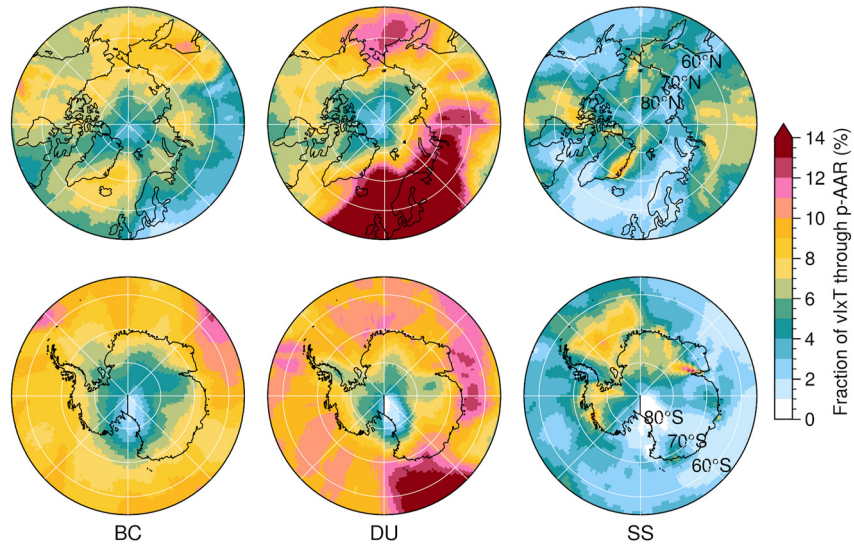

Figure A3. Importance of polar Aerosol Atmospheric Rivers for aerosol transport. Annual average fraction of poleward Black carbon (BC - left), Dust (DU - center) and Sea salt (SS - right) transport occurring through polar Aerosol Atmospheric River events for the period 1908–2022.

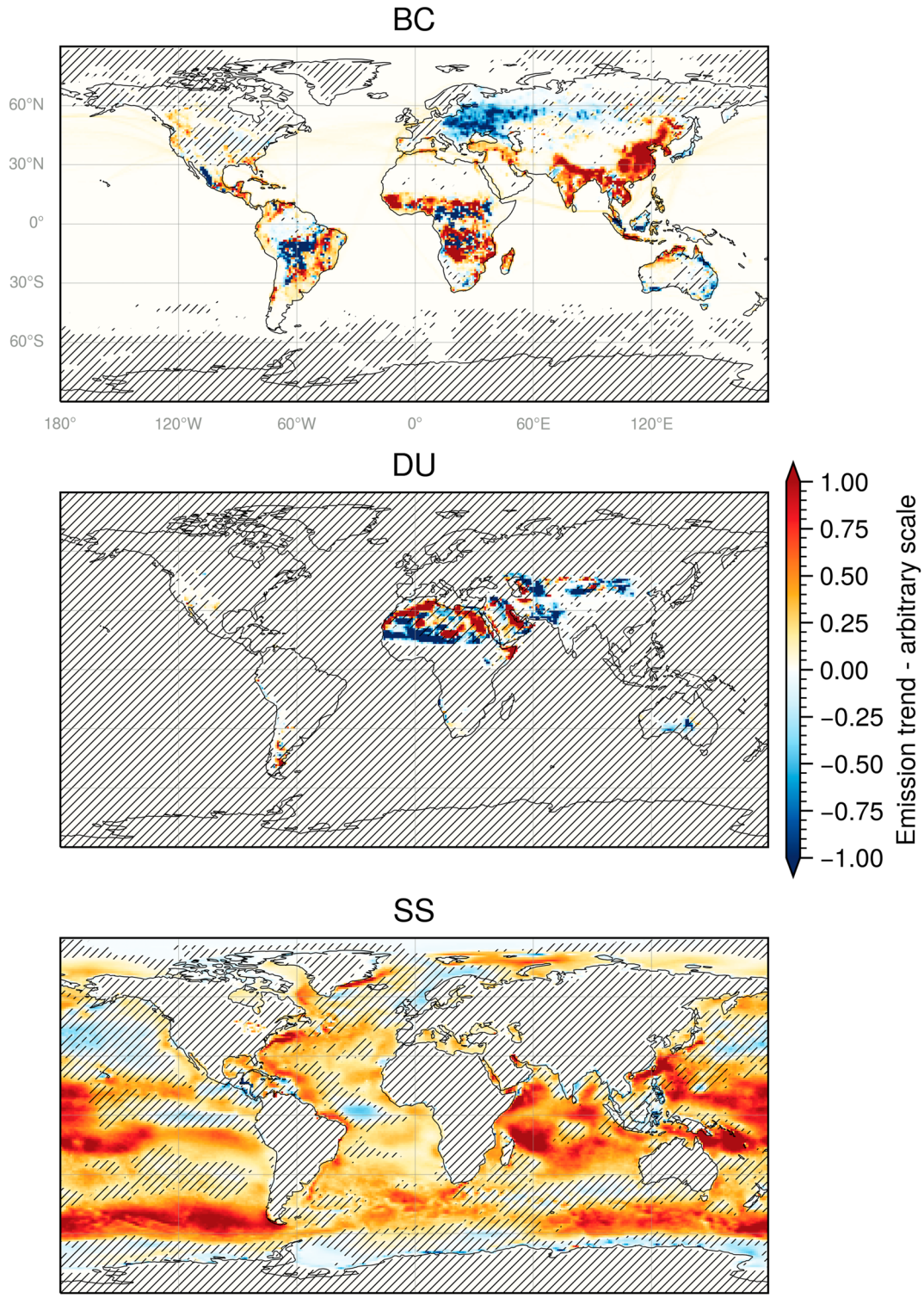

Figure A4. Aerosol emission trends. Trends in annual emissions of Black carbon (BC - top), Dust (DU - middle), Sea salt (SS - bottom) in MERRA-2 over the period 1980–2022. Hatching indicates non-significant trends at the 95% level based on a Mann-Kendall test.

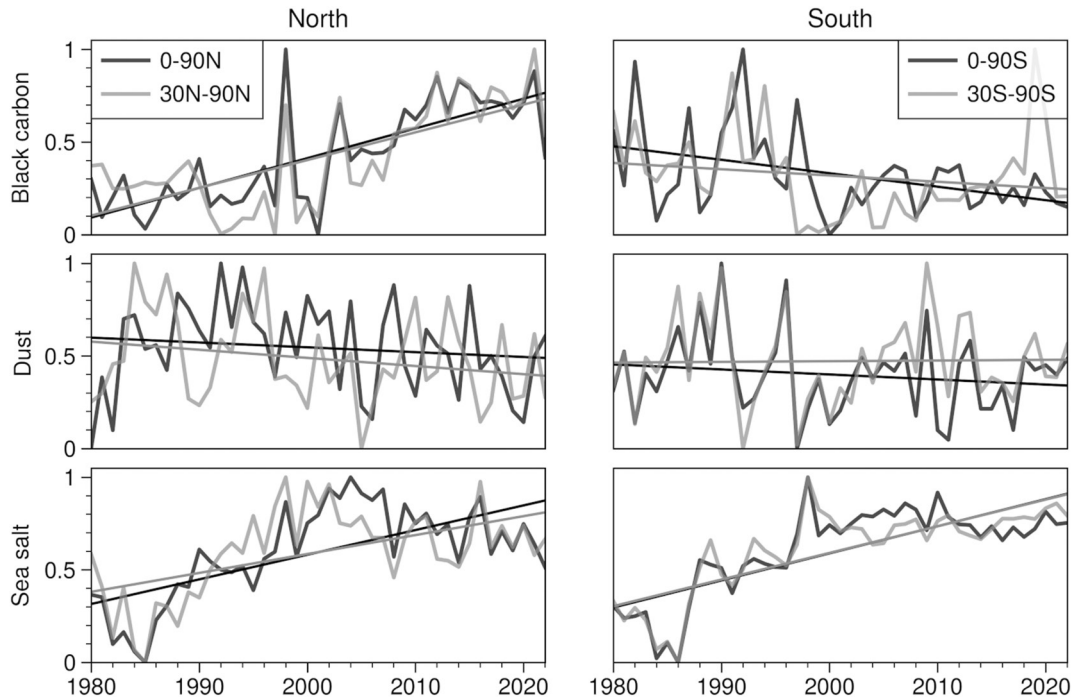

Figure A5. Aerosol emission trends. Sensitivity of emission trends to the cut-off latitude. Black is for a cut-off at the equator, gray is for a cut-off at 30°N-S.

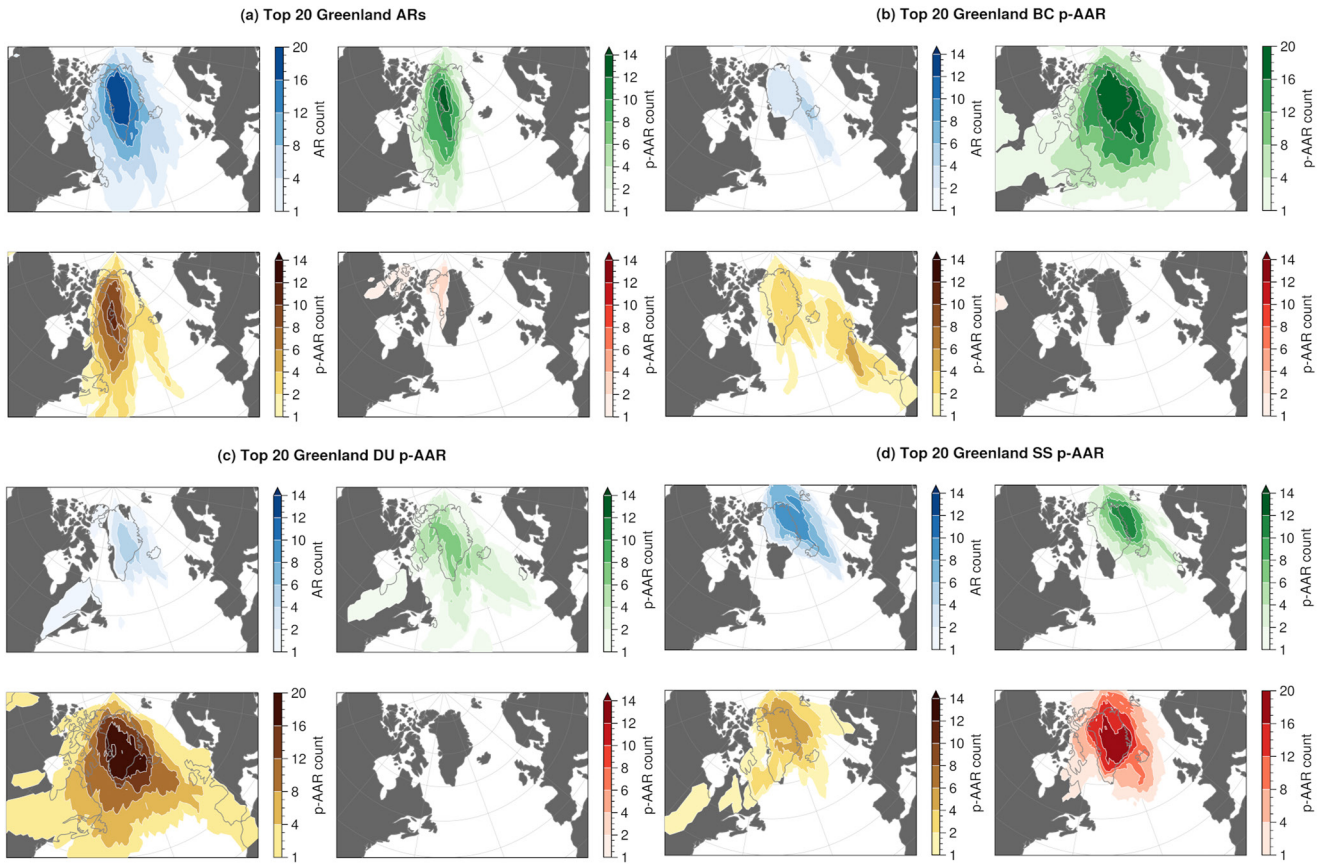

Figure A6. Top 20 Atmospheric Rivers and polar Aerosol Atmospheric Rivers in Greenland. Blue shades are Atmospheric Rivers (AR), green shades are Black carbon (BC) polar Aerosol Atmospheric Rivers (p-AAR), yellow shades are Dust (DU) p-AAR, red shades are Sea salt (SS) p-AAR. (a) Composite of the top 20 ARs in terms of cumulated meridional Integrated Vapor Transport (v*IVT*) reaching Greenland, and associated p-AARs. Panel (b) same as (a) but for the top 20 BC p-AAR. Panel (c) same as (b) but for DU p-AAR. Panel (d) same as (b) but for SS p-AAR. AR/p-AAR counts correspond to the number of AR/p-AAR days for the top 20 dates, for each grid point.

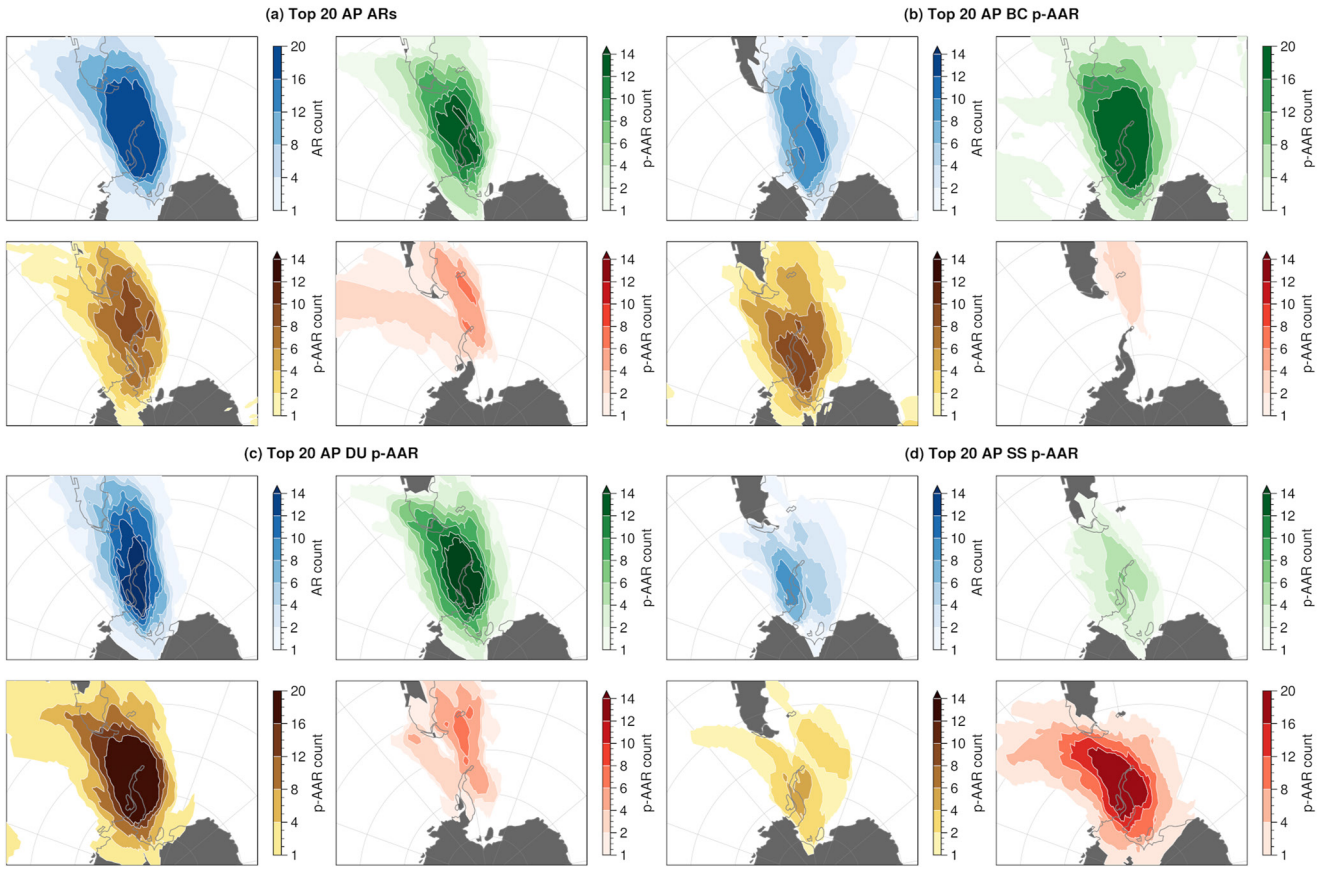

Figure A7. Top 20 Atmospheric Rivers and polar Aerosol Atmospheric Rivers in the Antarctic Peninsula. Same as Figure 10 but for Atmospheric Rivers and polar Aerosol Atmospheric Rivers reaching the Antarctic Peninsula.

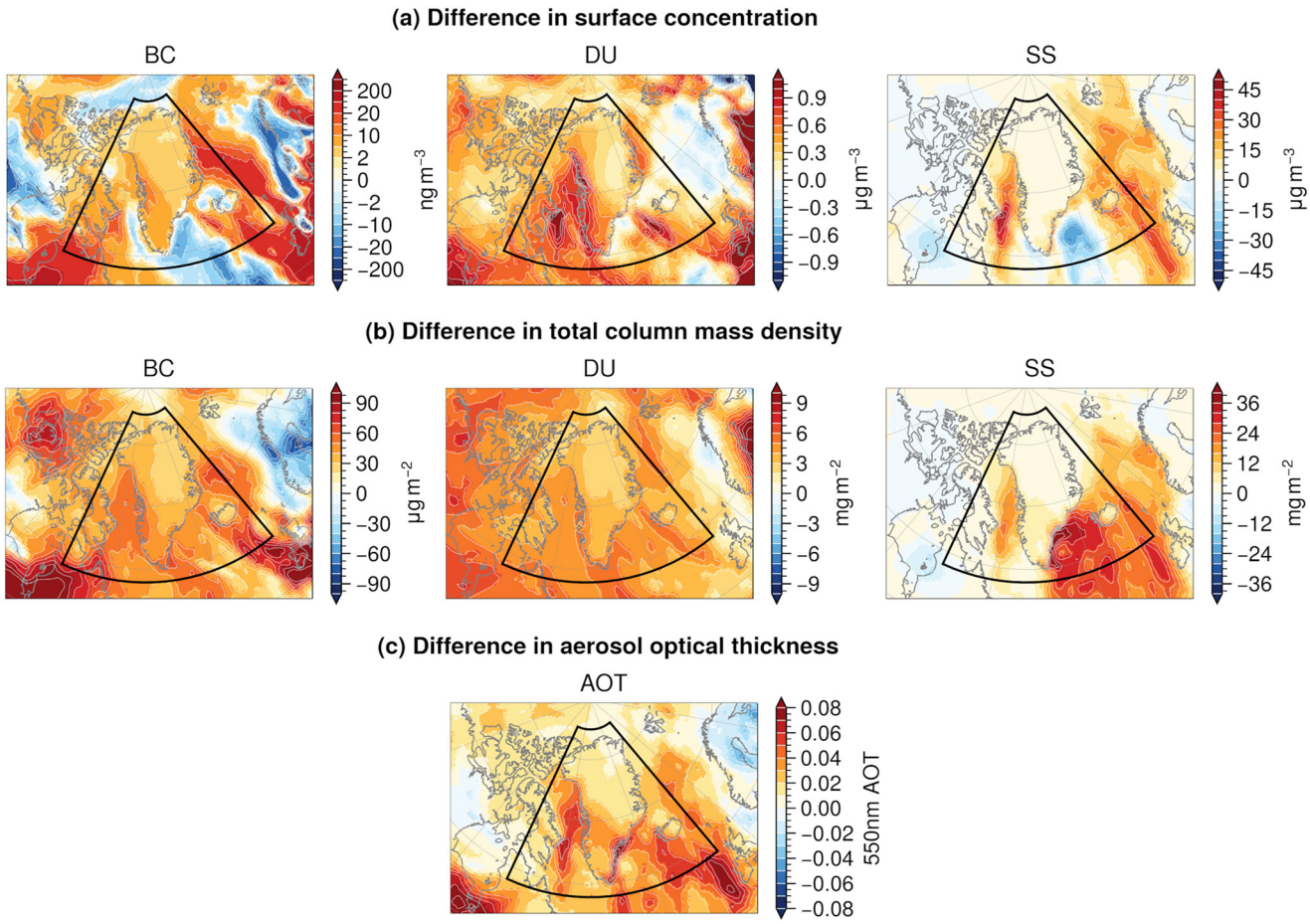

Figure A8. Effect of polar Aerosol Atmospheric Rivers on aerosol mass and optical properties. Difference in (a) surface mass concentration of Black carbon (BC), Dust (DU) and Sea salt (SS), (b) total column mass concentration of aerosols, and (c) total aerosol optical thickness (AOT), between days with combined Atmospheric River (AR) and polar Aerosol Atmospheric Rivers, and days with AR only. The days/area considered for compositing are the same as in Figures 11a and 11b.

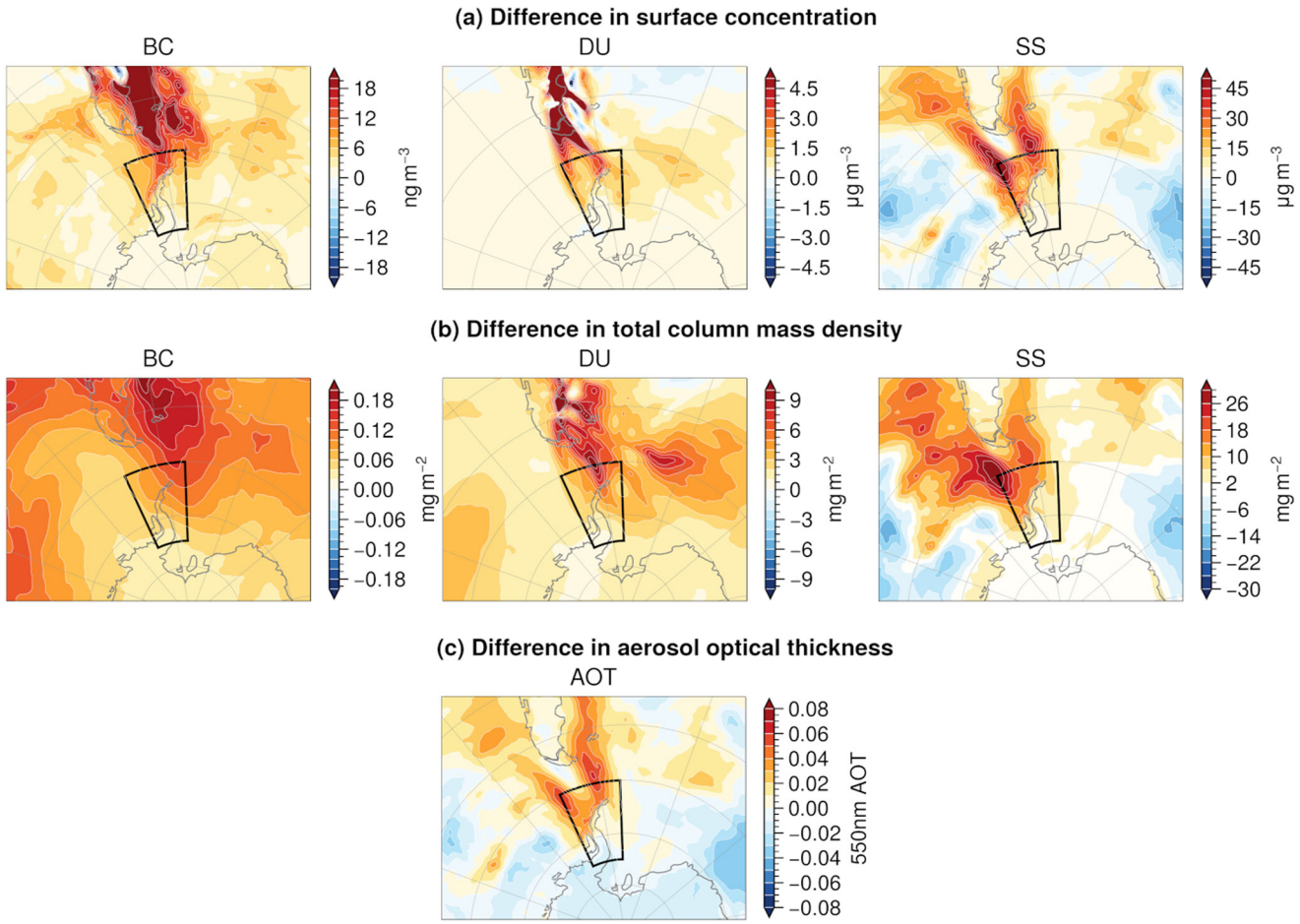

Figure A9. Same as Figure A8 but for Antarctic Peninsula events.

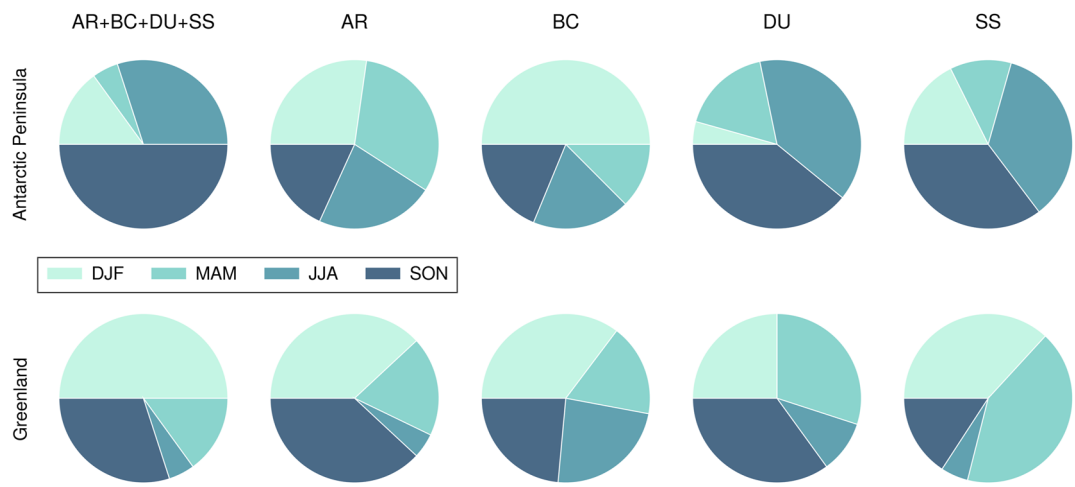

Figure A10. Seasonal distribution of the top 20 Atmospheric Rivers and polar Aerosol Atmospheric Rivers. Frequency of occurrence, by season, of the top 20 Atmospheric Rivers (AR) and Black carbon (BC), Dust (DU), Sea salt (SS) polar Aerosol Atmospheric Rivers (p-AAR) composites from Figure 11.

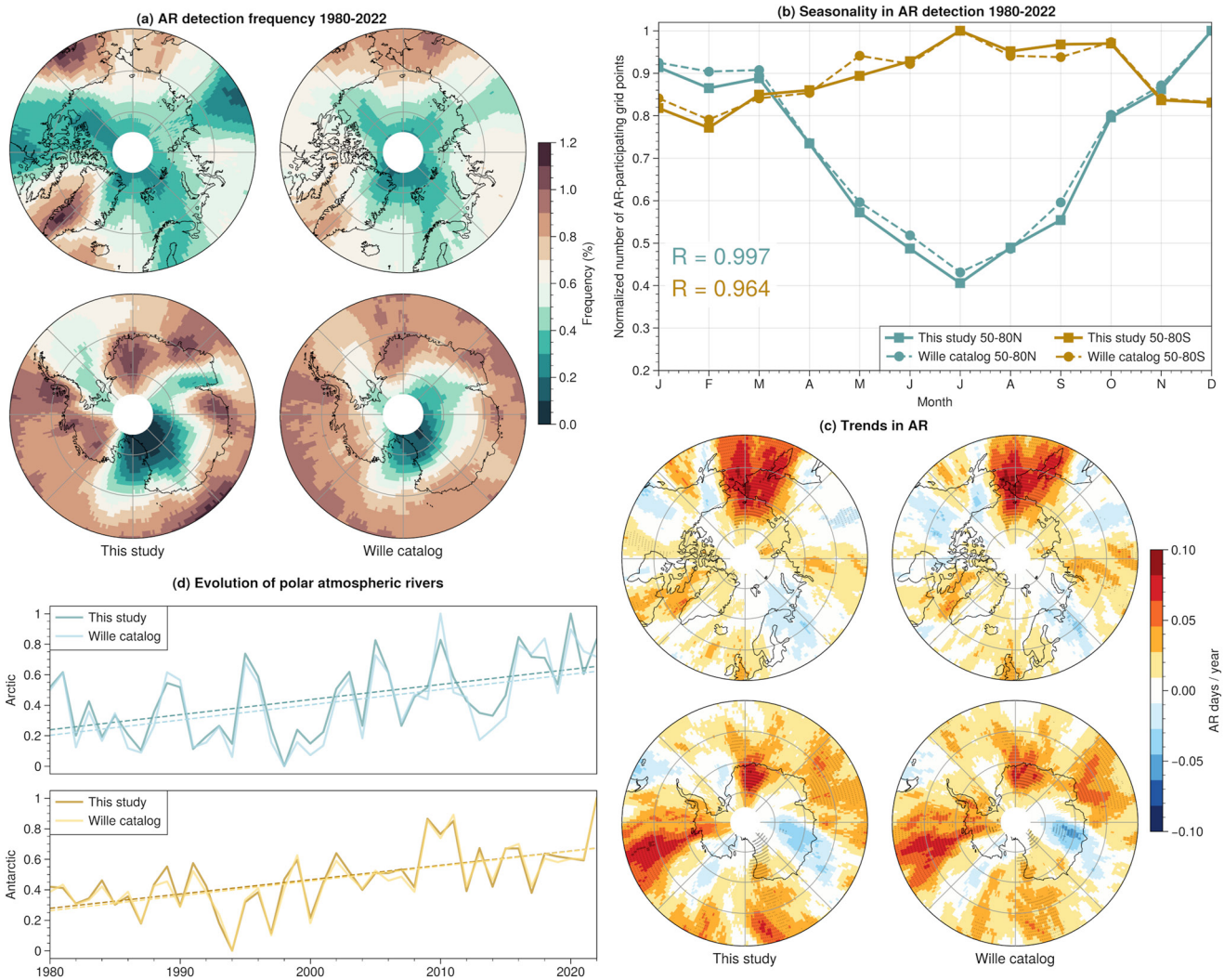

Figure A11. Validation of the adaptations made to the Wille et al. (2019) Atmospheric River detection scheme. (a) Frequency of Atmospheric River (AR) grid points detected in 1980–2022 using our method (left) and the Wille et al. (2019) method (right). (b) Seasonality in the normalized number of AR grid points in 1980–2022 above 50° N (blue) and below 50° S (gold), with our method (solid line) and the Wille et al. (2019) method (dashed line). Spatial averaging is weighted by the cell surface. R indicates the Pearson correlation coefficient between our catalog and the Wille et al. (2019) catalog. (c) Trends in AR days per year in the Antarctic, over the period 1980–2022, in this work (left) and in Wille et al. (2021) (right). (d) Relative evolution of AR frequency in the Arctic (top - 50–80° N) and Antarctic (bottom - 50–80° S) in both catalogs, for the period 1980–2022.

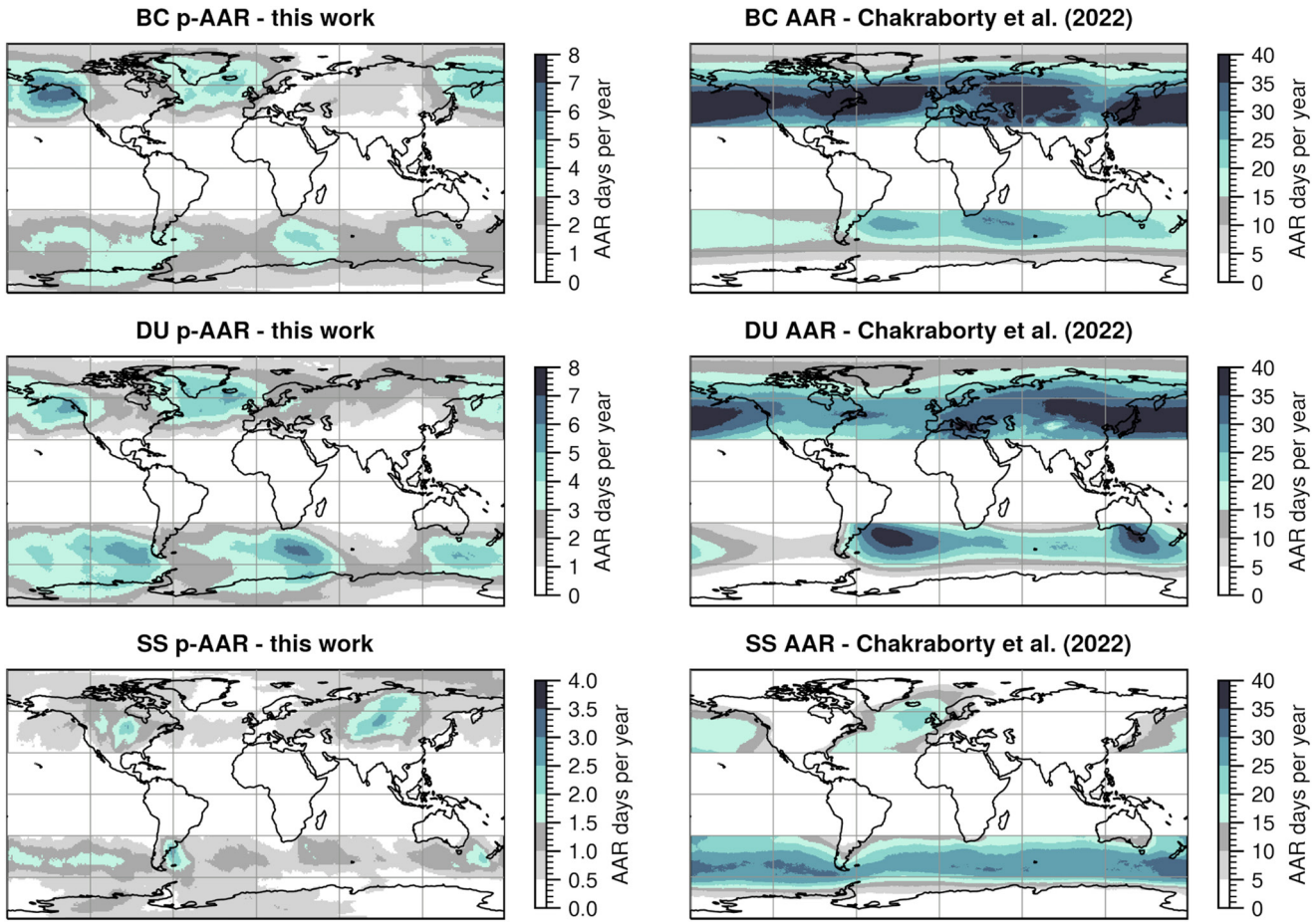

Figure A12. Climatology of polar Aerosol Atmospheric Rivers and Aerosol Atmospheric Rivers. Average annual frequency (in days per year) of Black carbon (BC), Dust (DU) and Sea salt (SS) polar Aerosol Atmospheric River (p-AAR) detection from this work (left) and Aerosol Atmospheric River detection (AAR) from Chakraborty (2022) (right). Period 1997–2014. Different scales are used for different panels.

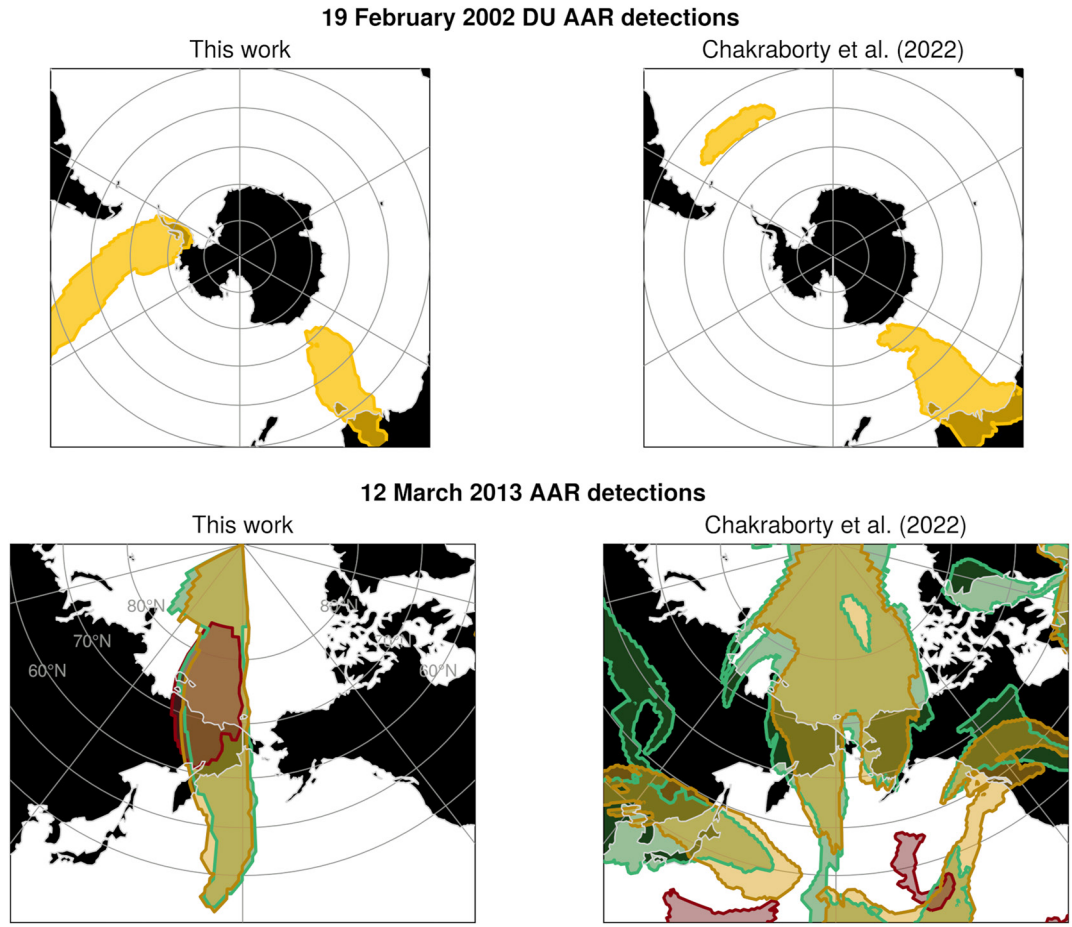

Figure A13. Polar Aerosol Atmospheric Rivers and Aerosol Atmospheric Rivers detection for two major events. Polar Aerosol Atmospheric River (p-AAR - left) and Aerosol Atmospheric River (AAR - right) detection from Chakraborty (2022) for two case studies presented in this work.

A2. Adaptations to and Validation of AR Detection

The method for the detection of ARs and p-AARs is based on the algorithm described in Wille et al. (2019, 2021). In this scheme, the criterion variable is the integrated meridional flux of water vapor (vIqT_{Wille}) between the 900 and 300 hPa pressure levels (Equation A1), taken every 3 hr.

$$\text{v}IqT_{\text{Wille}} = -\frac{1}{g}\int_{900\,hPa}^{300\,hPa} V\,q\,dp \tag{A1}$$

where V is the meridional wind, q is the water vapor mixing ratio, and dp is the pressure level increment. NB: Wille et al. (2019) apply a $-\frac{1}{g}$ factor, with g the gravity acceleration, for dimensional purposes. We do not apply this scaling factor in our detection because we are not interested in vIqT absolute values but only relative to the P97 threshold (which is not affected by a constant multiplicative factor).

Only poleward fluxes (i.e., V positive in the northern hemisphere, and V negative in the southern hemisphere) are considered. The threshold on vIqT_{Wille} is defined as the 98th percentile of vIqT_{Wille} (P98), computed for each month and each grid cell, over the 1980–2018 climatology. At each time step, if vIqT_{Wille} in a grid cell is above the corresponding month's threshold, the grid cell is counted as an AR-participating point. When an area of continuous AR-participating points is longer than 20° latitude, an AR is detected.

In this work, the detection algorithm differs from Wille et al. (2019) as follows. (a) While Wille et al. (2019) keep the original MERRA-2 resolution of 0.5° lat × 0.625° lon, our data is regridded to a 1° × 1° spatial resolution.

We perform this regridding for data storage management and because we foresee applications of our algorithm for global climate models, which tend to have a resolution closer to 1° × 1°, (b) instead of limiting the integral between 900 hPa and 300 hPa, the flux is taken for the whole column, in order to leverage the integrated variables provided by MERRA-2, and capture the aerosols present below 900 hPa and above 300 hPa identified in Figures 3 and A2. This can have an impact over land near the surface where katabatic winds may affect the flux (Wille et al., 2019). As a result, our criterion variable becomes v*IxT* as described by Equation 1. This v*IxT* is a pre-computed quantity provided by MERRA-2 as an integrated meridional flux. (c) As a result of the two previous differences, our threshold is taken as the P97 of v*IxT* instead of P98, in order to obtain similar climatologies as in Wille et al. (2019) as shown in Figure A11. (d) The climatology is updated and covers the period 1980–2022.

Our methodology for AR detection is slightly different from the Wille et al. (2019) algorithm, both in terms of input data, detection threshold, and implementation. Therefore a validation is carried out, comparing our results in terms of AR climatology and trends with those from the Wille et al. (2019) catalog. The detection catalog from Wille et al. (2019) covers the years 1980–2022 and is available through the ARTMIP database https://doi.org/10.5065/D62R3QFS (Rutz et al., 2019).

Figure A11 summarizes this comparison, with Figure A11a showing that, for the years 1980–2022, both methodologies yield similar magnitudes and spatial patterns in the frequency of AR detection both in the Arctic and the Antarctic, except for slightly stronger gradients in our detection. In the Arctic, maximum frequencies of around 1% are obtained over Greenland, coming from the Northwest Atlantic region, and in the Bering strait region, coming from the North Pacific, with an additional pathway over Western Russia. In the Antarctic, West Antarctica and the peninsula, along with Queen Maud Land feature a 1% maximum frequency detection in both catalogs. Furthermore, the underlying seasonality of ARs, aggregated by pole (50–80°N for the Arctic, 50–80°S for the Antarctic), is the same with both approaches, as described in Figure A11b, with monthly Pearson correlation coefficients of 0.99 and 0.96, for the Arctic and Antarctic, respectively, for the period 1980–2022. This seasonality is stronger in the Arctic with a maximum of detection in winter and a minimum in summer. A weaker seasonality with a maximum in austral winter is observed for the Antarctic.

In terms of trends, Figure A11c shows almost identical spatial patterns between the two catalogs. Both catalogs mainly show increasing trends in the regions where AR detection is climatologically most frequent, suggesting an amplification effect more than a change in physical processes. In the Arctic, the Bering strait region features the largest increasing trend with around 1 more AR day per decade. In the Antarctic, West Antarctica and Queen Maud land are the regions where this increasing trend is the most significant with also 1 more AR day per decade. Finally, Figure A11d describes this trend comparison in terms of regionally aggregated time series, showing very similar annual variations along with identical overall increasing trends over the 1980–2022 period.

In conclusion, despite slight methodological differences, the results given by our adapted polar AR detection scheme are very comparable to (Wille et al., 2019), and our detection leveraging vertically integrated variables provided by MERRA-2 is therefore fit for purpose and can be duplicated to aerosols.

Another parameter than the threshold percentile that could be tuned for p-AARs is the shape criterion imposing a minimum 20° extent in latitude. Aerosol sources, including anthropogenic activities and biomass burning, exist in North America and Siberia around 65°–70°N. Because of the 20°-latitude length criterion, p-AARs originating from these sources will not be accounted for unless they reach the pole. From an aerosol transport perspective this may seem like a limitation. However, we argue that, by design, p-AARs should generally detect extreme, long-range transport of background aerosols from the mid-latitudes, rather than relating to aerosol sources activity. In this respect, we believe it is relevant to keep the 20°-latitude length condition for aerosols as well, despite the implied rejection of high latitude sources that can be important for the Arctic aerosol budget. For the Antarctic, this criterion is not a problem since all aerosol sources (except sea salt) are further away than 20° in latitude.

A3. Comparison Between p-AARs and AARs

In the atmospheric river community, it has been demonstrated that the use of non-polar specific methods have important limitations for the detection of water vapor transport extremes to the poles (Collow et al., 2022; Shields et al., 2022), which is what motivated the use of a polar-adapted detection method here. Therefore, the detection

method for p-AAR used in this work is different from the approach by Chakraborty et al. (2021, 2022) for AAR. The main differences are summarized below:

- Chakraborty et al. (2021, 2022) use both zonal and meridional components, whereas our algorithm considers only the meridional component of the integrated transport. This choice is made following the findings from Wille et al. (2019, 2022) that for polar applications, the meridional wind speed component better reflects the dynamical processes that lead to precipitation generation, which is ultimately one of the important applications of this work.
- Chakraborty et al. (2021, 2022) use an aspect ratio criterion, which in our case is only a condition on latitudinal extent.
- Chakraborty et al. (2021, 2022) use a P85 detection threshold which is more permissive than our P97 threshold, which leads to a different event selection.

As a result of these methodological differences, the frequency of AAR detection is very different between our catalog and the one created by Chakraborty et al. (2021, 2022). Because they use a lower detection threshold (P85), and because both the meridional and zonal components are considered in their work, they detect more frequent AAR compared to our catalog. We have maximum frequencies of up to 8 BC and DU p-AAR days per year in the North Atlantic and North Pacific, where they obtain up to more than 40 BC or DU AAR days per year in these regions (Figure A12). Similarly, in the Antarctic 5 days per year is our maximum of detection frequency whereas they find up to 40 days per year of BC or DU AAR. In addition to different frequencies, the spatial patterns are also different.

Regarding two of the case studies presented in Section 3.2, the two approaches also result in different conclusions. The 2002 AP case does not appear as a DU AAR in Chakraborty et al. (2022), although a DU AAR is similarly detected between Australia and Antarctica (Figure A13). On the other hand, the 2013 Asia case shows many AARs (BC, DU and SS) detected on the day of the event in the Chakraborty et al. (2022) catalog, while our method shows one clear single event. The fact that these two events studied here, which had already been described as major transport events, were clearly detected as p-AARs and not so clearly as AARs proves that our classification makes sense and can be used for more systematic impact studies in polar regions.

Acknowledgments
This project has received funding from the European Union's Horizon 2020 research and innovation programme under grant agreement No 101003826 via project CRiceS (Climate Relevant interactions and feedbacks: the key role of sea ice and Snow in the polar and global climate system). VF and JW acknowledge support from the Agence Nationale de la Recherche project ANR-20CE01-0013 (ARCA). AE and PZ acknowledge the EU H2020 FORCeS project, contract No 821205. We acknowledge J. Schmale at École Polytechnique Fédérale de Lausanne and her team/collaborators who conducted the aerosol measurements during the international Multidisciplinary drifting Observatory for the Study of the Arctic Climate (MOSAiC). These data sets, already published in Dada et al. (2022), were used in this work for the validation of our methodology. We are grateful for their commitment to open data sharing, which advances scientific knowledge. RL, JT, JA and PZ acknowledge the course on "eScience Tools in Climate Science: Linking Observations with Modelling," which was held from 31 October to 11 November 2022 at Tjärnö Marine Laboratory, Sweden, and organized by Michael Schulz (MetNo, Norway) and Paul Zieger (SU, Sweden), for its inspiring atmosphere that contributed to some ideas of this work.

Data Availability Statement

The detection catalogs for AR and p-AAR, based on MERRA-2 vertically integrated fluxes at 1° × 1° spatial resolution and covering the period 1980–2022, along with the processing and detection codes, are available at https://doi.org/10.5281/zenodo.8082768 (Lapere, 2023).

References

Abbatt, J. P. D., Leaitch, W. R., Aliabadi, A. A., Bertram, A. K., Blanchet, J.-P., Boivin-Rioux, A., et al. (2019). Overview paper: New insights into aerosol and climate in the Arctic. *Atmospheric Chemistry and Physics*, *19*(4), 2527–2560. https://doi.org/10.5194/acp-19-2527-2019

Acosta Navarro, J. C., Varma, V., Riipinen, I., Seland, Ø., Kirkevåg, A., Struthers, H., et al. (2016). Amplification of arctic warming by past air pollution reductions in Europe. *Nature Geoscience*, *9*(4), 277–281. https://doi.org/10.1038/ngeo2673

Adusumilli, S., Fish, M. A., Fricker, H. A., & Medley, B. (2021). Atmospheric river precipitation contributed to rapid increases in surface height of the west Antarctic ice sheet in 2019. *Geophysical Research Letters*, *48*(5), e2020GL091076. https://doi.org/10.1029/2020GL091076

AMAP. (2021). *AMAP assessment 2021: Impacts of short-lived climate forcers on arctic climate, air quality, and human health (Tech. Rep.)*. Arctic Monitoring and Assessment Programme (AMAP).

Amino, T., Iizuka, Y., Matoba, S., Shimada, R., Oshima, N., Suzuki, T., et al. (2021). Increasing dust emission from ice free terrain in southeastern Greenland since 2000. *Polar Science*, *27*, 100599. https://doi.org/10.1016/j.polar.2020.100599

Backman, J., Schmeisser, L., & Asmi, E. (2021). Asian emissions explain much of the arctic black carbon events. *Geophysical Research Letters*, *48*(5), e2020GL091913. https://doi.org/10.1029/2020GL091913

Barrie, L. A. (1986). Arctic air pollution: An overview of current knowledge. *Atmospheric Environment*, *20*(4), 643–663. https://doi.org/10.1016/0004-6981(86)90180-0

Bintanja, R., van der Wiel, K., van der Linden, E. C., Reusen, J., Bogerd, L., Krikken, F., & Selten, F. M. (2020). Strong future increases in Arctic precipitation variability linked to poleward moisture transport. *Science Advances*, *6*(7), eaax6869. https://doi.org/10.1126/sciadv.aax6869

Bond, T. C., Doherty, S. J., Fahey, D. W., Forster, P. M., Berntsen, T., DeAngelo, B. J., et al. (2013). Bounding the role of black carbon in the climate system: A scientific assessment. *Journal of Geophysical Research: Atmospheres*, *118*(11), 5380–5552. https://doi.org/10.1002/jgrd.50171

Böö, S., Ekman, A. M. L., Svensson, G., & Devasthale, A. (2023). Transport of mineral dust into the arctic in two reanalysis datasets of atmospheric composition. *Tellus B: Chemical and Physical Meteorology*, *75*(1), 13–32. https://doi.org/10.16993/tellusb.1866

Box, J. E., Wehrlé, A., van As, D., Fausto, R. S., Kjeldsen, K. K., Dachauer, A., et al. (2022). Greenland ice sheet rainfall, heat and albedo feedback impacts from the mid-august 2021 atmospheric river. *Geophysical Research Letters*, *49*(11), e2021GL097356. https://doi.org/10.1029/2021GL097356

Boyer, M., Aliaga, D., Pernov, J. B., Angot, H., Quéléver, L. L. J., Dada, L., et al. (2023). A full year of aerosol size distribution data from the central Arctic under an extreme positive Arctic Oscillation: Insights from the Multidisciplinary drifting Observatory for the Study of Arctic Climate (MOSAiC) expedition. *Atmospheric Chemistry and Physics*, *23*(1), 389–415. https://doi.org/10.5194/acp-23-389-2023

Bradski, G. (2000). *The OpenCV library*. Dr. Dobb's Journal of Software Tools.

Buizert, C., Gkinis, V., Severinghaus, J. P., He, F., Lecavalier, B. S., Kindler, P., et al. (2014). Greenland temperature response to climate forcing during the last deglaciation. *Science*, *345*(6201), 1177–1180. https://doi.org/10.1126/science.1254961

Bullard, J. E., Baddock, M., Bradwell, T., Crusius, J., Darlington, E., Gaiero, D., et al. (2016). High-latitude dust in the Earth system. *Reviews of Geophysics*, *54*(2), 447–485. https://doi.org/10.1002/2016RG000518

Casado, M., Landais, A., Picard, G., Münch, T., Laepple, T., Stenni, B., et al. (2018). Archival processes of the water stable isotope signal in East Antarctic ice cores. *The Cryosphere*, *12*(5), 1745–1766. https://doi.org/10.5194/tc-12-1745-2018

Cauquoin, A., Werner, M., & Lohmann, G. (2019). Water isotopes – Climate relationships for the mid-Holocene and preindustrial period simulated with an isotope-enabled version of MPI-ESM. *Climate of the Past*, *15*(6), 1913–1937. https://doi.org/10.5194/cp-15-1913-2019

Chakraborty, S. (2022). Global aerosol atmospheric rivers database, version 1 [Dataset]. UCLA Dataverse. https://doi.org/10.25346/S6/CXO9PD

Chakraborty, S., Guan, B., Waliser, D. E., & da Silva, A. M. (2022). Aerosol atmospheric rivers: Climatology, event characteristics, and detection algorithm sensitivities. *Atmospheric Chemistry and Physics*, *22*(12), 8175–8195. https://doi.org/10.5194/acp-22-8175-2022

Chakraborty, S., Guan, B., Waliser, D. E., da Silva, A. M., Uluatam, S., & Hess, P. (2021). Extending the atmospheric river concept to aerosols: Climate and air quality impacts. *Geophysical Research Letters*, *48*(9), e2020GL091827. https://doi.org/10.1029/2020GL091827

Chin, M., Ginoux, P., Kinne, S., Torres, O., Holben, B. N., Duncan, B. N., et al. (2002). Tropospheric aerosol optical thickness from the GOCART model and comparisons with satellite and Sun photometer measurements. *Journal of the Atmospheric Sciences*, *59*(3), 461–483. https://doi.org/10.1175/1520-0469(2002)059⟨0461:TAOTFT⟩2.0.CO;2

Clem, K. R., Bozkurt, D., Kennett, D., King, J. C., & Turner, J. (2022). Central tropical Pacific convection drives extreme high temperatures and surface melt on the Larsen C Ice Shelf, Antarctic Peninsula. *Nature Communications*, *13*(1), 3906. https://doi.org/10.1038/s41467-022-31119-4

Collow, A. B. M., Shields, C. A., Guan, B., Kim, S., Lora, J. M., McClenny, E. E., et al. (2022). An overview of ARTMIP's tier 2 reanalysis intercomparison: Uncertainty in the detection of atmospheric rivers and their associated precipitation. *Journal of Geophysical Research: Atmospheres*, *127*(8), e2021JD036155. https://doi.org/10.1029/2021JD036155

Corbett, J. J., Lack, D. A., Winebrake, J. J., Harder, S., Silberman, J. A., & Gold, M. (2010). Arctic shipping emissions inventories and future scenarios. *Atmospheric Chemistry and Physics*, *10*(19), 9689–9704. https://doi.org/10.5194/acp-10-9689-2010

Creamean, J. M., Suski, K. J., Rosenfeld, D., Cazorla, A., DeMott, P. J., Sullivan, R. C., et al. (2013). Dust and biological aerosols from the Sahara and Asia influence precipitation in the Western U.S. *Science*, *339*(6127), 1572–1578. https://doi.org/10.1126/science.1227279

Dada, L., Angot, H., Beck, I., Baccarini, A., Quéléver, L. L. J., Boyer, M., et al. (2022). A central arctic extreme aerosol event triggered by a warm air-mass intrusion. *Nature Communications*, *13*(1), 1–15. https://doi.org/10.1038/s41467-022-32872-2

Eastman, R., & Warren, S. G. (2010). Interannual variations of arctic cloud types in relation to sea ice. *Journal of Climate*, *23*(15), 4216–4232. https://doi.org/10.1175/2010JCLI3492.1

Francis, D., Fonseca, R., Nelli, N., Bozkurt, D., Picard, G., & Guan, B. (2022). Atmospheric rivers drive exceptional Saharan dust transport towards Europe. *Atmospheric Research*, *266*, 105959. https://doi.org/10.1016/j.atmosres.2021.105959

Frey, M. M., Norris, S. J., Brooks, I. M., Anderson, P. S., Nishimura, K., Yang, X., et al. (2020). First direct observation of sea salt aerosol production from blowing snow above sea ice. *Atmospheric Chemistry and Physics*, *20*(4), 2549–2578. https://doi.org/10.5194/acp-20-2549-2020

Gershunov, A., Shulgina, T., Ralph, F. M., Lavers, D. A., & Rutz, J. J. (2017). Assessing the climate-scale variability of atmospheric rivers affecting western north America. *Geophysical Research Letters*, *44*(15), 7900–7908. https://doi.org/10.1002/2017GL074175

Global Modeling and Assimilation Office (GMAO). (2015a). MERRA-2 inst3_3d_aer_Nv: 3d,3-Hourly,Instantaneous,Model-Level,Assimilation,Aerosol Mixing Ratio V5.12.4 [Dataset]. Goddard Earth Sciences Data and Information Services Center (GES DISC). https://doi.org/10.5067/LTVB4GPCOTK2

Global Modeling and Assimilation Office (GMAO). (2015b). MERRA-2 tavg1_2d_aer_Nx: 2d,1-Hourly,Time-averaged,Single-Level,Assimilation,Aerosol Diagnostics V5.12.4 [Dataset]. Goddard Earth Sciences Data and Information Services Center (GES DISC). https://doi.org/10.5067/KLICLTZ8EM9D

Global Modeling and Assimilation Office (GMAO). (2015c). MERRA-2 tavg1_2d_int_Nx: 2d,1-Hourly,Time-Averaged,Single-Level,Assimilation,Vertically Integrated Diagnostics V5.12.4 [Dataset]. Goddard Earth Sciences Data and Information Services Center (GES DISC). https://doi.org/10.5067/Q5GVUVUIVGO7

Global Modeling and Assimilation Office (GMAO). (2015d). MERRA-2 tavg1_2d_slv_Nx: 2d,1-Hourly,Time-Averaged,Single-Level,Assimilation,Single-Level Diagnostics V5.12.4 [Dataset]. Goddard Earth Sciences Data and Information Services Center (GES DISC). https://doi.org/10.5067/VJAFPLI1CSIV

Global Modeling and Assimilation Office (GMAO). (2015e). MERRA-2 tavgM_2d_adg_Nx: 2d,Monthly mean,Time-averaged,Single-Level,Assimilation,Aerosol Diagnostics (extended) V5.12.4 [Dataset]. Goddard Earth Sciences Data and Information Services Center (GES DISC). https://doi.org/10.5067/RZIK2TV7PP38

Gorodetskaya, I., Tsukernik, M., Claes, K., Ralph, M. F., Neff, W. D., & Van Lipzig, N. P. M. (2014). The role of atmospheric rivers in anomalous snow accumulation in east Antarctica. *Geophysical Research Letters*, *41*(17), 6199–6206. https://doi.org/10.1002/2014GL060881

Goursaud, S., Masson-Delmotte, V., Favier, V., Preunkert, S., Legrand, M., Minster, B., & Werner, M. (2019). Challenges associated with the climatic interpretation of water stable isotope records from a highly resolved firn core from Adélie Land, coastal Antarctica. *The Cryosphere*, *13*(4), 1297–1324. https://doi.org/10.5194/tc-13-1297-2019

Hall, A. (2004). The role of surface albedo feedback in climate. *Journal of Climate*, *17*(7), 1550–1568. https://doi.org/10.1175/1520-0442(2004)017⟨1550:TROSAF⟩2.0.CO;2

Held, I. M., & Soden, B. J. (2006). Robust responses of the hydrological cycle to global warming. *Journal of Climate*, *19*(21), 5686–5699. https://doi.org/10.1175/JCLI3990.1

Heutte, B., Beck, I., Quéléver, L., Jokinen, T., Laurila, T., Dada, L., & Schmale, J. (2022). Equivalent black carbon concentration in 10 minutes time resolution, measured in the Swiss container during MOSAiC 2019/2020 [Dataset]. PANGAEA. https://doi.org/10.1594/PANGAEA.952251

Hunter, J. D. (2007). Matplotlib: A 2D graphics environment. *Computing in Science & Engineering*, *9*(3), 90–95. https://doi.org/10.1109/MCSE.2007.55

Ikeda, K., Tanimoto, H., Sugita, T., Akiyoshi, H., Kanaya, Y., Zhu, C., & Taketani, F. (2017). Tagged tracer simulations of black carbon in the arctic: Transport, source contributions, and budget. *Atmospheric Chemistry and Physics*, *17*(17), 10515–10533. https://doi.org/10.5194/acp-17-10515-2017

Irish, V. E., Hanna, S. J., Willis, M. D., China, S., Thomas, J. L., Wentzell, J. J. B., et al. (2019). Ice nucleating particles in the marine boundary layer in the canadian arctic during summer 2014. *Atmospheric Chemistry and Physics*, *19*(2), 1027–1039. https://doi.org/10.5194/acp-19-1027-2019

Jouzel, J., Alley, R. B., Cuffey, K. M., Dansgaard, W., Grootes, P., Hoffmann, G., et al. (1997). Validity of the temperature reconstruction from water isotopes in ice cores. *Journal of Geophysical Research*, *102*(C12), 26471–26487. https://doi.org/10.1029/97JC01283

Jumelet, J., Klekociuk, A. R., Alexander, S. P., Bekki, S., Hauchecorne, A., Vernier, J. P., et al. (2020). Detection of aerosols in Antarctica from long-range transport of the 2009 Australian wildfires. *Journal of Geophysical Research: Atmospheres*, *125*(23), e2020JD032542. https://doi.org/10.1029/2020JD032542

Kawai, K., Matsui, H., & Tobo, Y. (2023). Dominant role of arctic dust with high ice nucleating ability in the arctic lower troposphere. *Geophysical Research Letters*, *50*(8), e2022GL102470. https://doi.org/10.1029/2022GL102470

Kirpes, R. M., Bonanno, D., May, N. W., Fraund, M., Barget, A. J., Moffet, R. C., et al. (2019). Wintertime Arctic sea spray aerosol composition controlled by sea ice lead microbiology. *ACS Central Science*, *5*(11), 1760–1767. https://doi.org/10.1021/acscentsci.9b00541

Kluyver, T., Ragan-Kelley, B., Pérez, F., Granger, B., Bussonnier, M., Frederic, J., et al. (2016). Jupyter notebooks – A publishing format for reproducible computational workflows. In F. Loizides & B. Schmidt (Eds.), *Positioning and power in academic publishing: Players, agents and agendas* (pp. 87–90).

Komatsu, K. K., Alexeev, V. A., Repina, I. A., & Tachibana, Y. (2018). Poleward upgliding Siberian atmospheric rivers over sea ice heat up Arctic upper air. *Scientific Reports*, *8*(1), 2872. https://doi.org/10.1038/s41598-018-21159-6

Krinner, G., & Genthon, C. (2003). Tropospheric transport of continental tracers towards Antarctica under varying climatic conditions. *Tellus B: Chemical and Physical Meteorology*, *55*(1), 54–70. https://doi.org/10.1034/j.1600-0889.2003.00004.x

Krinner, G., & Werner, M. (2003). Impact of precipitation seasonality changes on isotopic signals in polar ice cores: A multi-model analysis. *Earth and Planetary Science Letters*, *216*(4), 525–538. https://doi.org/10.1016/S0012-821X(03)00550-8

Lachlan-Cope, T. (2010). Antarctic clouds. *Polar Research*, *29*(2), 150–158. https://doi.org/10.3402/polar.v29i2.6065

Lapere, R. (2023). Polar atmospheric and aerosol river detection catalogs [Dataset/Software]. Zenodo. https://doi.org/10.5281/zenodo.8082768

Lapere, R., Thomas, J. L., Marelle, L., Ekman, A. M. L., Frey, M. M., Lund, M. T., et al. (2023). The representation of sea salt aerosols and their role in polar climate within CMIP6. *Journal of Geophysical Research: Atmospheres*, *128*(6), e2022JD038235. https://doi.org/10.1029/2022JD038235

Lavers, D. A., Villarini, G., Allan, R. P., Wood, E. F., & Wade, A. J. (2012). The detection of atmospheric rivers in atmospheric reanalyses and their links to British winter floods and the large-scale climatic circulation. *Journal of Geophysical Research*, *117*, D20. https://doi.org/10.1029/2012JD018027

Lenaerts, J. T. M., Medley, B., van den Broeke, M. R., & Wouters, B. (2019). Observing and modeling ice sheet surface mass balance. *Reviews of Geophysics*, *57*(2), 376–420. https://doi.org/10.1029/2018RG000622

Levine, J. G., Yang, X., Jones, A. E., & Wolff, E. W. (2014). Sea salt as an ice core proxy for past sea ice extent: A process-based model study. *Journal of Geophysical Research: Atmospheres*, *119*(9), 5737–5756. https://doi.org/10.1002/2013JD020925

Li, F., Ginoux, P., & Ramaswamy, V. (2008). Distribution, transport, and deposition of mineral dust in the southern ocean and Antarctica: Contribution of major sources. *Journal of Geophysical Research*, *113*(D10). https://doi.org/10.1029/2007JD009190

Maclennan, M. L., & Lenaerts, J. T. M. (2021). Large-scale atmospheric drivers of snowfall over Thwaites glacier, Antarctica. *Geophysical Research Letters*, *48*(17), e2021GL093644. https://doi.org/10.1029/2021GL093644

Maclennan, M. L., Lenaerts, J. T. M., Shields, C. A., Hoffman, A. O., Wever, N., Thompson-Munson, M., et al. (2023). Climatology and surface impacts of atmospheric rivers on West Antarctica. *The Cryosphere*, *17*(2), 865–881. https://doi.org/10.5194/tc-17-865-2023

Marelle, L., Raut, J.-C., Law, K. S., & Duclaux, O. (2018). Current and future arctic aerosols and ozone from remote emissions and emerging local sources—Modeled source contributions and radiative effects. *Journal of Geophysical Research: Atmospheres*, *123*(22), 12942–12963. https://doi.org/10.1029/2018JD028863

Mattingly, K. S., Mote, T. L., & Fettweis, X. (2018). Atmospheric river impacts on Greenland ice sheet surface mass balance. *Journal of Geophysical Research: Atmospheres*, *123*(16), 8538–8560. https://doi.org/10.1029/2018JD028714

Matus, A. V., & L'Ecuyer, T. S. (2017). The role of cloud phase in Earth's radiation budget. *Journal of Geophysical Research: Atmospheres*, *122*(5), 2559–2578. https://doi.org/10.1002/2016JD025951

Mei, L., Xue, Y., de Leeuw, G., von Hoyningen-Huene, W., Kokhanovsky, A. A., Istomina, L., et al. (2013). Aerosol optical depth retrieval in the Arctic region using MODIS data over snow. *Remote Sensing of Environment*, *128*, 234–245. https://doi.org/10.1016/j.rse.2012.10.009

Meinander, O., Dagsson-Waldhauserova, P., Amosov, P., Aseyeva, E., Atkins, C., Baklanov, A., et al. (2022). Newly identified climatically and environmentally significant high-latitude dust sources. *Atmospheric Chemistry and Physics*, *22*(17), 11889–11930. https://doi.org/10.5194/acp-22-11889-2022

Moseid, K. O., Schulz, M., Eichler, A., Schwikowski, M., McConnell, J. R., Olivié, D., et al. (2022). Using ice cores to evaluate CMIP6 aerosol concentrations over the historical era. *Journal of Geophysical Research: Atmospheres*, *127*(18), e2021JD036105. https://doi.org/10.1029/2021JD036105

Murray, B. J., Carslaw, K. S., & Field, P. R. (2021). Opinion: Cloud-phase climate feedback and the importance of ice-nucleating particles. *Atmospheric Chemistry and Physics*, *21*(2), 665–679. https://doi.org/10.5194/acp-21-665-2021

Murray, B. J., O'Sullivan, D., Atkinson, J. D., & Webb, M. E. (2012). Ice nucleation by particles immersed in supercooled cloud droplets. *Chemical Society Reviews*, *41*(19), 6519–6554. https://doi.org/10.1039/C2CS35200A

Myhre, G., Shindell, D., Bréon, F.-M., Collins, W., Fuglestvedt, J., Huang, J., et al. (2013). In T. F. Stocker, D. Qin, G.-K. Plattner, M. Tignor, S. K. Allen, J. Boschung, et al. (Eds.), *Climate change 2013: The physical science basis. Contribution of working Group I to the fifth assessment report of the intergovernmental panel on climate change*, *In (chap. Anthropogenic and natural radiative forcing)*. Cambridge University Press.

NASA. (2013). EOSDIS Worldview. Retrieved from https://worldview.earthdata.nasa.gov/

Nash, D., Waliser, D., Guan, B., Ye, H., & Ralph, F. M. (2018). The role of atmospheric rivers in extratropical and polar hydroclimate. *Journal of Geophysical Research: Atmospheres*, *123*(13), 6804–6821. https://doi.org/10.1029/2017JD028130

Neff, P. D., & Bertler, N. A. N. (2015). Trajectory modeling of modern dust transport to the southern ocean and Antarctica. *Journal of Geophysical Research: Atmospheres*, *120*(18), 9303–9322. https://doi.org/10.1002/2015JD023304

Neiman, P. J., Ralph, F. M., Moore, B. J., Hughes, M., Mahoney, K. M., Cordeira, J. M., & Dettinger, M. D. (2013). The landfall and inland penetration of a flood-producing atmospheric river in Arizona. Part I: Observed synoptic-scale, orographic, and hydrometeorological characteristics. *Journal of Hydrometeorology*, *14*(2), 460–484. https://doi.org/10.1175/JHM-D-12-0101.1

Nygård, T., Naakka, T., & Vihma, T. (2020). Horizontal moisture transport dominates the regional moistening patterns in the Arctic. *Journal of Climate*, *33*(16), 6793–6807. https://doi.org/10.1175/JCLI-D-19-0891.1

O'Brien, T. A., Wehner, M. F., Payne, A. E., Shields, C. A., Rutz, J. J., Leung, L.-R., et al. (2022). Increases in future AR count and size: Overview of the ARTMIP Tier 2 CMIP5/6 experiment. *Journal of Geophysical Research: Atmospheres*, *127*(6), e2021JD036013. https://doi.org/10.1029/2021JD036013

Papritz, L., Hauswirth, D., & Hartmuth, K. (2022). Moisture origin, transport pathways, and driving processes of intense wintertime moisture transport into the Arctic. *Weather and Climate Dynamics*, *3*, 1–20. https://doi.org/10.5194/wcd-3-1-2022

Pernov, J. B., Beddows, D., Thomas, D. C., Dall´Osto, M., Harrison, R. M., Schmale, J., et al. (2022). Increased aerosol concentrations in the High Arctic attributable to changing atmospheric transport patterns. *npj Climate and Atmospheric Science*, *5*(1), 1–13. https://doi.org/10.1038/s41612-022-00286-y

Pithan, F., Svensson, G., Caballero, R., Chechin, D., Cronin, T. W., Ekman, A. M. L., et al. (2018). Role of air-mass transformations in exchange between the Arctic and mid-latitudes. *Nature Geoscience*, *11*(11), 805–812. https://doi.org/10.1038/s41561-018-0234-1

Pohl, B., Favier, V., Wille, J., Udy, D. G., Vance, T. R., Pergaud, J., et al. (2021). Relationship between weather regimes and atmospheric Rivers in East Antarctica. *Journal of Geophysical Research: Atmospheres*, *126*(24), e2021JD035294. https://doi.org/10.1029/2021JD035294

Quinn, P. K., Shaw, G., Andrews, E., Dutton, E. G., Ruoho-Airola, T., & Gong, S. L. (2007). Arctic haze: Current trends and knowledge gaps. *Tellus B: Chemical and Physical Meteorology*, *59*(1), 99–114. https://doi.org/10.1111/j.1600-0889.2006.00238.x

Quinn, P. K., Stohl, A., Arneth, A., Berntsen, T., Burkhart, J. F., Christensen, J., et al. (2011). The impact of black carbon on arctic climate. *Arctic Monitoring and Assessment Programme (AMAP)*.

Ralph, F. M., Rutz, J. J., Cordeira, J. M., Dettinger, M., Anderson, M., Reynolds, D., et al. (2019). A scale to characterize the strength and impacts of atmospheric rivers. *Bulletin of the American Meteorological Society*, *100*(2), 269–289. https://doi.org/10.1175/BAMS-D-18-0023.1

Randles, C. A., Da Silva, A. M., Buchard, V., Colarco, P. R., Darmenov, A., Govindaraju, R., et al. (2017). The MERRA-2 aerosol reanalysis, 1980 – Onward, Part I: System description and data assimilation evaluation. *Journal of Climate*, *30*(17), 6823–6850. https://doi.org/10.1175/JCLI-D-16-0609.1

Rantanen, M., Karpechko, A. Y., Lipponen, A., Nordling, K., Hyvärinen, O., Ruosteenoja, K., et al. (2022). The Arctic has warmed nearly four times faster than the globe since 1979. *Communications Earth & Environment*, *3*, 1–10. https://doi.org/10.1038/s43247-022-00498-3

Raut, J.-C., Marelle, L., Fast, J. D., Thomas, J. L., Weinzierl, B., Law, K. S., et al. (2017). Cross-polar transport and scavenging of Siberian aerosols containing black carbon during the 2012 ACCESS summer campaign. *Atmospheric Chemistry and Physics*, *17*(18), 10969–10995. https://doi.org/10.5194/acp-17-10969-2017

Rhodes, R. H., Yang, X., & Wolff, E. W. (2018). Sea ice versus storms: What controls sea salt in arctic ice cores? *Geophysical Research Letters*, *45*(11), 5572–5580. https://doi.org/10.1029/2018GL077403

Rinke, A., Segger, B., Crewell, S., Maturilli, M., Naakka, T., Nygård, T., et al. (2019). Trends of vertically integrated water vapor over the arctic during 1979–2016: Consistent moistening all over? *Journal of Climate*, *32*(18), 6097–6116. https://doi.org/10.1175/JCLI-D-19-0092.1

Roiger, A., Schlager, H., Schäfler, A., Huntrieser, H., Scheibe, M., Aufmhoff, H., et al. (2011). In-situ observation of Asian pollution transported into the Arctic lowermost stratosphere. *Atmospheric Chemistry and Physics*, *11*(21), 10975–10994. https://doi.org/10.5194/acp-11-10975-2011

Roiger, A., Thomas, J.-L., Schlager, H., Law, K. S., Kim, J., Schäfler, A., et al. (2015). Quantifying emerging local anthropogenic emissions in the arctic region: The ACCESS aircraft campaign experiment. *Bulletin of the American Meteorological Society*, *96*(3), 441–460. https://doi.org/10.1175/BAMS-D-13-00169.1

Rutz, J. J., Shields, C. A., Lora, J. M., Payne, A. E., Guan, B., Ullrich, P. A., et al. (2019). Artmip tier-1 catalogues [Dataset]. UCAR. https://doi.org/10.5065/D62R3QFS

Schmale, J., Zieger, P., & Ekman, A. M. L. (2021). Aerosols in current and future Arctic climate. *Nature Climate Change*, *11*(2), 95–105. https://doi.org/10.1038/s41558-020-00969-5

Servettaz, A. P. M., Orsi, A. J., Curran, M. A. J., Moy, A. D., Landais, A., McConnell, J. R., et al. (2023). A 2000-year temperature reconstruction on the East Antarctic plateau from argon–nitrogen and water stable isotopes in the Aurora Basin North ice core. *Climate of the Past*, *19*(6), 1125–1152. https://doi.org/10.5194/cp-19-1125-2023

Shi, Y., Liu, X., Wu, M., Zhao, X., Ke, Z., & Brown, H. (2022). Relative importance of high-latitude local and long-range-transported dust for Arctic ice-nucleating particles and impacts on Arctic mixed-phase clouds. *Atmospheric Chemistry and Physics*, *22*(4), 2909–2935. https://doi.org/10.5194/acp-22-2909-2022

Shields, C. A., Payne, A. E., Shearer, E. J., Wehner, M. F., O'Brien, T. A., Rutz, J. J., et al. (2023). Future atmospheric rivers and impacts on precipitation: Overview of the ARTMIP tier 2 high-resolution global warming experiment. *Geophysical Research Letters*, *50*(6), e2022GL102091. https://doi.org/10.1029/2022GL102091

Shields, C. A., Rosenbloom, N., Bates, S., Hannay, C., Hu, A., Payne, A. E., et al. (2019). Meridional heat transport during atmospheric rivers in high-resolution CESM climate projections. *Geophysical Research Letters*, *46*(24), 14702–14712. https://doi.org/10.1029/2019GL085565

Shields, C. A., Rutz, J. J., Leung, L.-Y., Ralph, F. M., Wehner, M., Kawzenuk, B., et al. (2018). Atmospheric river tracking method intercomparison project (ARTMIP): Project goals and experimental design. *Geoscientific Model Development*, *11*(6), 2455–2474. https://doi.org/10.5194/gmd-11-2455-2018

Shields, C. A., Wille, J. D., Marquardt Collow, A. B., Maclennan, M., & Gorodetskaya, I. V. (2022). Evaluating uncertainty and modes of variability for Antarctic atmospheric rivers. *Geophysical Research Letters*, *49*(16), e2022GL099577. https://doi.org/10.1029/2022GL099577

Shupe, M. D., Rex, M., Blomquist, B., Persson, P. O. G., Schmale, J., Uttal, T., et al., (2022). Overview of the MOSAiC expedition: Atmosphere. *Elementa: Science of the Anthropocene*, *10*(1), 00060. https://doi.org/10.1525/elementa.2021.00060

Skiles, S. M., Flanner, M., Cook, J. M., Dumont, M., & Painter, T. H. (2018). Radiative forcing by light-absorbing particles in snow. *Nature Climate Change*, *8*(11), 964–971. https://doi.org/10.1038/s41558-018-0296-5

Sodemann, H., Pommier, M., Arnold, S. R., Monks, S. A., Stebel, K., Burkhart, J. F., et al. (2011). Episodes of cross-polar transport in the Arctic troposphere during July 2008 as seen from models, satellite, and aircraft observations. *Atmospheric Chemistry and Physics*, *11*(8), 3631–3651. https://doi.org/10.5194/acp-11-3631-2011

Stohl, A. (2006). Characteristics of atmospheric transport into the Arctic troposphere. *Journal of Geophysical Research*, *111*(D11), D11306. https://doi.org/10.1029/2005JD006888

Szopa, S., Naik, V., Adhikary, B., Artaxo, P., Berntsen, T., Collins, W., et al. (2021). In V. Masson-Delmotte, P. Zhai, A. Pirani, S. L. Connors, C. Pean, S. Berger, et al. (Eds.), *Climate change 2021: The physical science basis. Contribution of working Group I to the sixth assessment report of the intergovernmental panel on climate change*, *In (chap. Short-lived climate forcers)*. Cambridge University Press. https://doi.org/10.1017/9781009157896.008

Tan, I., & Storelvmo, T. (2019). Evidence of strong contributions from mixed-phase clouds to arctic climate change. *Geophysical Research Letters*, *46*(5), 2894–2902. https://doi.org/10.1029/2018GL081871

Thomas, J. L., Polashenski, C. M., Soja, A. J., Marelle, L., Casey, K. A., Choi, H. D., et al. (2017). Quantifying black carbon deposition over the Greenland ice sheet from forest fires in Canada. *Geophysical Research Letters*, *44*(15), 7965–7974. https://doi.org/10.1002/2017GL073701

Thomas, M. A., Devasthale, A., Tjernström, M., & Ekman, A. M. L. (2019). The relation between aerosol vertical distribution and temperature inversions in the Arctic in winter and spring. *Geophysical Research Letters*, *46*(5), 2836–2845. https://doi.org/10.1029/2018GL081624

Turner, J., Phillips, T., Hosking, J. S., Marshall, G. J., & Orr, A. (2013). The Amundsen sea low. *International Journal of Climatology*, *33*(7), 1818–1829. https://doi.org/10.1002/joc.3558

Turner, J., Phillips, T., Thamban, M., Rahaman, W., Marshall, G. J., Wille, J. D., et al. (2019). The dominant role of extreme precipitation events in Antarctic snowfall variability. *Geophysical Research Letters*, *46*(6), 3502–3511. https://doi.org/10.1029/2018GL081517

Wahl, S., Steen-Larsen, H. C., Hughes, A. G., Dietrich, L. J., Zuhr, A., Behrens, M., et al. (2022). Atmosphere-snow exchange explains surface snow isotope variability. *Geophysical Research Letters*, *49*(20), e2022GL099529. https://doi.org/10.1029/2022GL099529

Wang, H., Rasch, P. J., Easter, R. C., Singh, B., Zhang, R., Ma, P.-L., et al. (2014). Using an explicit emission tagging method in global modeling of source-receptor relationships for black carbon in the arctic: Variations, sources, and transport pathways. *Journal of Geophysical Research: Atmospheres*, *119*(22), 12888–12909. https://doi.org/10.1002/2014JD022297

Wendisch, M., Brückner, M., Crewell, S., Ehrlich, A., Notholt, J., Lüpkes, C., et al. (2023). Atmospheric and surface processes, and feedback mechanisms determining arctic amplification: A review of first results and prospects of the (AC)3 project. *Bulletin of the American Meteorological Society*, *104*(1), E208–E242. https://doi.org/10.1175/BAMS-D-21-0218.1

Werner, M., Heimann, M., & Hoffmann, G. (2001). Isotopic composition and origin of polar precipitation in present and glacial climate simulations. *Tellus B: Chemical and Physical Meteorology*, *53*(1), 53–71. https://doi.org/10.3402/tellusb.v53i1.16539

Wille, J. D., Favier, V., Dufour, A., Gorodetskaya, I. V., Turner, J., Agosta, C., & Codron, F. (2019). West Antarctic surface melt triggered by atmospheric rivers. *Nature Geoscience*, *12*(11), 911–916. https://doi.org/10.1038/s41561-019-0460-1

Wille, J. D., Favier, V., Gorodetskaya, I. V., Agosta, C., Kittel, C., Beeman, J. C., et al. (2021). Antarctic atmospheric river climatology and precipitation impacts. *Journal of Geophysical Research: Atmospheres*, *126*(8), e2020JD033788. https://doi.org/10.1029/2020JD033788

Wille, J. D., Favier, V., Jourdain, N. C., Kittel, C., Turton, J. V., Agosta, C., et al. (2022). Intense atmospheric rivers can weaken ice shelf stability at the Antarctic Peninsula. *Communications Earth & Environment*, *3*, 1–14. https://doi.org/10.1038/s43247-022-00422-9

Wolff, E. W., Fischer, H., Fundel, F., Ruth, U., Twarloh, B., Littot, G. C., et al. (2006). Southern Ocean sea-ice extent, productivity and iron flux over the past eight glacial cycles. *Nature*, *440*(7083), 491–496. https://doi.org/10.1038/nature04614

Xian, P., Zhang, J., O'Neill, N. T., Toth, T. D., Sorenson, B., Colarco, P. R., et al. (2022). Arctic spring and summertime aerosol optical depth baseline from long-term observations and model reanalyses – Part 1: Climatology and trend. *Atmospheric Chemistry and Physics*, *22*(15), 9915–9947. https://doi.org/10.5194/acp-22-9915-2022

Xu, J.-W., Martin, R. V., Morrow, A., Sharma, S., Huang, L., Leaitch, W. R., et al. (2017). Source attribution of Arctic black carbon constrained by aircraft and surface measurements. *Atmospheric Chemistry and Physics*, *17*(19), 11971–11989. https://doi.org/10.5194/acp-17-11971-2017

Yang, X., Pyle, J. A., & Cox, R. A. (2008). Sea salt aerosol production and bromine release: Role of snow on sea ice. *Geophysical Research Letters*, *35*(16), L16815. https://doi.org/10.1029/2008GL034536

You, C., Tjernström, M., Devasthale, A., & Steinfeld, D. (2022). The role of atmospheric blocking in regulating arctic warming. *Geophysical Research Letters*, *49*(12), e2022GL097899. https://doi.org/10.1029/2022GL097899

Yun, J., Evoy, E., Worthy, S. E., Fraser, M., Veber, D., Platt, A., et al. (2022). Ice nucleating particles in the Canadian high arctic during the fall of 2018. *Environmental Sciences: Atmosphere*, *2*(2), 279–290. https://doi.org/10.1039/D1EA00068C

Zamora, L. M., Kahn, R. A., Evangeliou, N., Groot Zwaaftink, C. D., & Huebert, K. B. (2022). Comparisons between the distributions of dust and combustion aerosols in MERRA-2, FLEXPART, and CALIPSO and implications for deposition freezing over wintertime Siberia. *Atmospheric Chemistry and Physics*, *22*(18), 12269–12285. https://doi.org/10.5194/acp-22-12269-2022

Zhang, P., Chen, G., Ting, M., Ruby Leung, L., Guan, B., & Li, L. (2023). More frequent atmospheric rivers slow the seasonal recovery of Arctic sea ice. *Nature Climate Change*, *13*(3), 266–273. https://doi.org/10.1038/s41558-023-01599-3

Zhao, X., Huang, K., Fu, J. S., & Abdullaev, S. F. (2022). Long-range transport of Asian dust to the Arctic: Identification of transport pathways, evolution of aerosol optical properties, and impact assessment on surface albedo changes. *Atmospheric Chemistry and Physics*, *22*(15), 10389–10407. https://doi.org/10.5194/acp-22-10389-2022

Zhou, Y., Wu, T., Zhou, Y., Zhang, J., Zhang, F., Su, X., et al. (2023). Can global warming bring more dust? *Climate Dynamics*, *61*(5–6), 2693–2715. https://doi.org/10.1007/s00382-023-06706-w

Zhu, Y., & Newell, R. E. (1998). A proposed algorithm for moisture fluxes from atmospheric rivers. *Monthly Weather Review*, *126*(3), 725–735. https://doi.org/10.1175/1520-0493(1998)126⟨0725:APAFMF⟩2.0.CO;2

Zieger, P., Heslin-Rees, D., Karlsson, L., Koike, M., Modini, R., & Krejci, R. (2023). Black carbon scavenging by low-level arctic clouds. *Nature Communications*, *14*(1), 5488. https://doi.org/10.1038/s41467-023-41221-w